

Impact of scalar NSI on the neutrino mass ordering sensitivity at DUNE, HK and KNO

Arnab Sarker,^{a,1} Abinash Medhi,^{a,2} Dharitree Bezboruah,^{a,3} Moon Moon Devi,^{a,4} and Debajyoti Dutta^{b,5}

^a*Department of Physics, Tezpur University, Napaam, Sonitpur, Assam-784028, India*

^b*Department of Physics, Assam Don Bosco University, Kamarkuchi, Sonapur, Assam-782402, India*

E-mail: ¹arnabs@tezu.ernet.in, ²amedhi@tezu.ernet.in,
³dbbphy1@tezu.ernet.in, ⁴devimm@tezu.ernet.in,
⁵debajyoti.dutta@dbuniversity.ac.in

ABSTRACT: The study of neutrino non-standard interactions (NSI) is a well-motivated phenomenological scenario to explore new physics beyond the Standard Model. The possible scalar coupling of neutrinos (ν) with matter is one of such new physics scenarios that appears as a sub-dominant effect that can impact the ν -oscillations in matter. The presence of scalar NSI introduces an additional contribution directly to the ν -mass matrix in the interaction Hamiltonian and subsequently to the ν -oscillations. This indicates that scalar NSI may have a significant impact on measurements related to ν -oscillations e.g. leptonic CP phase (δ_{CP}), θ_{23} octant and neutrino mass ordering (MO). The linear scaling of the effects of scalar NSI with matter density also motivates its exploration in long-baseline (LBL) experiments. In this paper, we study the impact of a scalar-mediated NSI on the MO sensitivity of DUNE, HK and HK+KNO, which are upcoming LBL experiments. We study the impact on MO sensitivities at these experiments assuming that scalar NSI parameters are present in nature and is known from other non-LBL experiments. We observe that the presence of diagonal scalar NSI elements can significantly affect the ν -mass ordering sensitivities. We then also combine the data from DUNE with HK and HK+KNO to explore possible synergy among these experiments in a wider parameter space. We also observe a significant enhancement in the MO sensitivities for the combined analysis.

KEYWORDS: Non-Standard Interactions, Neutrino Mass Ordering, Neutrino Physics, Beyond Standard Model, Long Baseline Experiments

Contents

1	Introduction	1
2	Formalism of Scalar NSI	5
3	Methodology	7
3.1	Simulation Details	7
3.2	Overview of the three LBL experiments	8
3.2.1	DUNE	8
3.2.2	HK	8
3.2.3	HK+KNO	8
4	Results and Discussion	9
4.1	Effects on the appearance channel $P_{\mu e}$	9
4.2	Imprints on the MO asymmetry	11
4.3	Impact on the MO sensitivities	13
4.4	The MO sensitivity for the Synergy of the LBL experiments	16
4.4.1	Combining DUNE with HK	17
4.4.2	Combining DUNE with HK+KNO	18
4.5	Precision measurement of Δm_{31}^2	19
5	Summary and concluding remarks	20

1 Introduction

The Standard Model (SM) of particle physics stands as one of the most successful theories to explain the fundamental nature of our universe. Still, there exist various phenomena that cannot be explained by theories within the SM, such as the phenomenon of ν -oscillations, the presence of dark matter and dark energy, baryon asymmetry etc. This compels us to explore physics beyond the Standard Model (BSM). Neutrino oscillations decisively affirm the existence of non-zero masses for neutrinos, marking the initial experimental indication of BSM physics [1, 2]. The current & upcoming ν -experiments are primarily focused on determining the three major unknowns in the neutrino sector viz. neutrino mass ordering (MO), octant of θ_{23} & leptonic CP phase. The various sub-dominant non-standard effects, like non-standard interactions (NSI) [3–37], Lorentz invariance violation (LIV) [38–51], neutrino decay [52–57], neutrino decoherence [58–62] etc., are also being explored through these experiments. The precise determination of the unknowns is of immense significance for the complete understanding of the standard 3ν paradigm. The presence of NSI may affect the physics sensitivities of these experiments. In this study, we have mainly focused

on exploring the impact of a scalar-mediated NSI on the MO sensitivities in the LBL sector, in a model-independent way. In our study, we include the upcoming LBL experiments namely DUNE, HK and HK+KNO. We have also performed a combined analysis of the MO sensitivities for DUNE with HK/HK+KNO.

The neutrino mass eigenstates may be defined in different ways, as described in the references [63–65]. In this work, we adopt the formalism such that the condition $|U_{e1}| > |U_{e2}| > |U_{e3}|$ holds true. The ordering of the absolute neutrino masses (m_1, m_2, m_3) are not yet fully known, where m_1 , m_2 and m_3 are the mass eigenstates. From the solar sector, we know that $m_2 > m_1$ [1, 66–68], however, the relative ordering of m_3 is yet to be determined. We have two possible ordering of ν -masses i.e. Normal Ordering (NO) ($m_3 > m_2 > m_1$) and Inverted Ordering (IO) ($m_2 > m_1 > m_3$) [69]. Various current and upcoming ν -experiments from the solar [66, 70–74], atmospheric [75–79], reactor [80–83] and LBL accelerator [84–90] sectors are equipped with advanced technologies and systematics which are expected to be highly sensitive to MO determination using different oscillation channels. The global analysis of neutrino oscillation data from LBL (T2K + NO ν A), reactor (Daya Bay, RENO, Double Chooz) and atmospheric (Super-K) sectors prefers NO over IO at 2.7σ Confidence Level (CL) as shown in reference [69]. In the current precision era, the future experiments are designed to have much higher sensitivities towards MO determination. All these experiments can individually achieve 3σ CL in MO determination [87, 88, 91–94]. In addition, combining experiments from different sectors can further enhance the sensitivities by leveraging the synergy and a wider parameter space. In the reference [95], the determination of neutrino mass ordering using disappearance channel independent of matter effects and via a combination of different experiments are discussed. The authors have shown that highly precise measurements of atmospheric mass splitting in ν_e and ν_μ disappearance channels can determine the mass ordering from the comparison of the location of the minima. They have compared for different choices of atmospheric Δm^2 . In [26], the MO sensitivity up to 15σ is obtained for synergy among T2HK, HK and DUNE. Combining current experiments T2K and NO ν A with DUNE and ESS ν SB, a 5σ sensitivity for ordering determination is obtained in [96]. A combination of T2K-II, NO ν A and JUNO can also provide a similar sensitivity, as studied in reference [97]. In [98], the authors have explored the MO sensitivity at INO-ICAL and have also performed a combined analysis with T2K, NO ν A and reactor experiments. Combining JUNO with IceCube Upgrade, and PINGU can also enhance the ordering sensitivity [99]. In reference [100], the MO sensitivity by combining JUNO and T2HK is studied. Though, JUNO alone has the potential of discovering MO at 3σ CL with 3% energy resolution, a synergy between JUNO and T2HK increases it up to 9σ . A synergy among T2HK, JUNO and atmospheric ν -experiment INO-ICAL also has the potential of determining the MO with up to 7σ CL with 5% energy resolution of JUNO [101].

Moreover, the MO sensitivities may be substantially affected by various BSM physics scenarios which makes it crucial to explore and understand such subdominant effects. In reference [102, 103], the data from the ongoing LBL experiments T2K and NO ν A are fitted in the presence of vector NSI. The inclusion of vector NSI has completely washed out the preference for NO as expected in the standard scenario. In reference [104], the

MO sensitivity and discovery potential, in the presence of vector NSI, are studied for the accelerator experiments T2K and NO ν A along with DUNE. The presence of vector NSI has a significant impact on the MO sensitivity. The sensitivity to mass ordering at 5σ CL is observed in DUNE for most values of δ_{CP} except for the case when ϵ_{ee} is negative. In presence of vector NSI, oscillation experiments alone can not determine the neutrino MO and θ_{12} octant due to the existence of exact degeneracy known as the LMA-Dark [105–107]. Scattering experiments, primarily coherent elastic neutrino-nucleus scattering (CE ν NS) and CE ν NS data from reactor experiments can break this degeneracy for mediator mass up to a few MeVs [35, 108]. The generalized MO degeneracy in the presence of vector NSI [9] deteriorates the ordering sensitivities of all three LBL experiments T2HK, T2HKK and DUNE as shown in the study [3]. In [19], the authors have studied the effect of vector NSI on the MO sensitivities, considering the diagonal NSI parameter ϵ_{ee} to be equal to -1 so that it can nullify the standard matter effect. In this scenario, if additionally δ_{CP} is $\pm\pi/2$, there will be an intrinsic degeneracy between MO and NSI that cannot be lifted even if we can precisely measure the values of ϵ_{ee} and δ_{CP} . Apart from vector NSI, other BSM phenomena can also affect the MO determination in LBL experiments. In reference [109], the authors have discussed how the non-unitarity in the ν -mixing matrix can affect MO determination in the accelerator experiments DUNE, NO ν A and T2K. The non-unitary mixing is found to decrease the MO sensitivity of these experiments. Though, DUNE will be sensitive to mass ordering discrimination even in the presence of non-unitarity for some values of δ_{CP} ; its sensitivity mostly decreases. In the case of NO ν A and T2K, the scenario worsens as a result of their shorter baseline and less matter interaction contribution. The MO sensitivity of DUNE, T2HK and T2HKK in a $(3 + 1)$ scenario, with one sterile neutrino is studied in [110]. The MO sensitivity deteriorates for small mixing with the sterile neutrino, but with increasing sterile mixing the MO sensitivity improves for all the experiments. The impact of various BSM physics scenarios on the MO sensitivities has been well explored for various LBL ν -experiments. Long-baseline accelerator experiments will provide the best measurement of Δm_{31}^2 . Note that, the presence of new physics can impact the measurement of $|\Delta m_{31}^2|$ as well as the determination of neutrino MO. The presence of SNSI in nature would be no exception. In this paper, we particularly probe the impact of diagonal scalar NSI elements on the MO sensitivities in the context of upcoming LBL experiments. We also perform a combined analysis for a chosen combination of LBL experiments as it can lead to increased statistics and broader parameter space. It may also help in better constraining the oscillation parameters.

The study of scalar NSI is a well-motivated phenomenological scenario to probe new physics searches in the leptonic sector. The possible scalar coupling of neutrinos with environmental fermions can modify the ν -oscillation probabilities and also affect the physics sensitivities of various ν -oscillation experiments [111–114]. This kind of unique coupling can manifest as medium-dependent corrections directly to the ν -mass matrix. Scalar NSI can be a unique probe to explore new physics phenomena in the neutrino sector. The effects of scalar NSI show a linear scaling relationship with environmental matter density, which makes LBL experiments a promising candidate for probing its effects.

At present, there are no stringent experimental bounds on the scalar NSI $\eta_{\alpha\beta}$ pa-

rameters. The reference [111] has shown a preliminary attempt at estimating scalar NSI parameter using data from Borexino. It suggests a preference for the scalar NSI parameter η_{ee} to be -0.16, specifically within the context of the solar sector, which of course needs to be translated by the density of the ratio. Considering the wide range of the Sun's density from 10^2 to 10^{-2} over the Sun's radius, we may approximately translate the η to obtain a range of η_{ee} from $\sim[-0.004, -0.464]$, if the Earth's density is fixed at $\rho = 2.9g/cc$. It may be noted that, the fit shown in [111] is rather naive, and further investigation using data from various experiments would be required for a clearer picture.

The values of $\eta_{\alpha\beta}$ that we use in our study serve solely as illustrative examples, allowing us to examine how scalar NSI influences the sensitivities of neutrino mass ordering across various long-baseline experiments. As the scalar NSI would be a sub-dominant effect, the modified Hamiltonian is expected to be a small perturbation to the original Hamiltonian. Some studies like [115, 116] have put bounds on the scalar NSI parameters under astrophysical and cosmological limits, although they are not so stringent. The authors in reference [117, 118] have explored the impact of scalar NSI on the CP-measurement sensitivities at DUNE and have also performed a combined analysis with T2HK and T2HKK. In reference [119], the authors have investigated various new physics scenarios in LBL experiments (NOvA, T2K and DUNE) and have found that in many cases DUNE will have better model discrimination. The authors in reference [120] have studied the effects of scalar NSI on the determination of CP-violation, θ_{23} octant and MO in the context of P2SO and DUNE. In reference [28], we have constrained the lightest ν -mass in the presence of scalar NSI as it has a direct dependence on the absolute ν -mass.

In this paper, we have explored the impact of scalar-mediated NSI on the neutrino MO sensitivity at the LBL experiments i.e. DUNE, HK (a.k.a. T2HK) and HK+KNO (a.k.a. T2HKK). We study the impact on mass ordering sensitivities at these experiments assuming that scalar NSI parameters are present in nature and are known from other non-LBL experiments. We have considered flavor conserving texture of scalar NSI and probed the impact of diagonal scalar NSI elements ($\eta_{ee}, \eta_{\mu\mu}, \eta_{\tau\tau}$) on the MO sensitivities for the chosen LBL experiments by taking only one element at a time. We find that the presence of scalar NSI can significantly improve/deteriorate the MO sensitivity of LBL experiments. A positive η_{ee} , mostly enhances the MO sensitivity as compared to the standard case for all three experiments. In this study, for the first time, we have performed an MO analysis in the presence of scalar NSI with the synergy of experiments viz. DUNE+HK and DUNE+HK+KNO. For the combined analysis of experiments, the overall MO sensitivities have significantly improved. It can also help in resolving underlying degeneracy in MO determination in the presence of scalar NSI. This is expected as the synergy of the experiments improves the statistics as well as widens the parameter region of the analysis. Currently, most of the ν -experiments aim at determining the neutrino MO unambiguously. The determination of neutrino MO is crucial as it would help us to understand the nature of neutrinos and could also provide insights into the origin of ν -mass.

The paper is organized into different sections as follows. We first discuss the formalism of scalar NSI in section 2. The methodology and experimental details of the analysis have been described in section 3. We present our findings, along with associated discussions, in

section 4. We then summarise the study in section 5.

2 Formalism of Scalar NSI

In SM, neutrinos interact with the environmental fermions by weak interactions while passing through matter. These interactions can either be charged-current (CC) type, mediated by a W^\pm or neutral-current (NC) type, mediated by a Z^0 boson [121]. The CC interactions can affect ν -oscillations by introducing a flavor-dependent matter potential, whereas NC interactions are flavor-independent and do not affect the ν -oscillations. Therefore, the effective Lagrangian for standard matter effect in ν -oscillations can be written as [122–126],

$$\mathcal{L}_{CC}^{eff} = -\frac{4G_F}{\sqrt{2}} [\bar{\nu}_e(p_3)\gamma_\mu P_L \nu_e(p_2)] [\bar{e}(p_1)\gamma^\mu P_L e(p_4)]. \quad (2.1)$$

In equation 2.1, G_F is the Fermi coupling constant, $P_L = (1 - \gamma_5)/2$ is the chiral projection operator for left-handed neutrinos and p_i 's are momenta of incoming and outgoing fermions as well as neutrino states. Therefore, the effective Hamiltonian for matter-effect in ν -oscillations expressed in flavor basis is,

$$\mathcal{H}_{matter} = E_\nu + \frac{MM^\dagger}{2E_\nu} \pm V_{SI}. \quad (2.2)$$

In equation 2.2, V_{SI} is the matter potential with positive and negative signs indicating neutrinos and anti-neutrinos respectively. E_ν is the energy of neutrinos. M is the ν -mass matrix in flavor basis, which is given by $\mathcal{U}D_\nu\mathcal{U}^\dagger$, where $D_\nu = \text{diag}(m_1, m_2, m_3)$ i.e. the diagonal mass matrix of neutrinos. \mathcal{U} is the PMNS mixing matrix [127–130]. The effective Hamiltonian can be simplified to the following form in terms of the mass-squared differences ($\Delta m_{ij}^2 = m_i^2 - m_j^2$) as

$$\mathcal{H}_{eff} = E_\nu + \frac{1}{2E_\nu} \mathcal{U} \cdot \text{diag}(0, \Delta m_{21}^2, \Delta m_{31}^2) \cdot \mathcal{U}^\dagger + \text{diag}(V_{CC}, 0, 0). \quad (2.3)$$

In BSM scenarios, the vector-mediated NSI has been extensively explored in the past few years. However, the possibility of NSIs mediated by a scalar particle is another intriguing scenario, which has very compelling phenomenological consequences. The effective Lagrangian for ν -fermion coupling mediated by a scalar particle, ϕ having mass m_ϕ is,

$$\mathcal{L}_{eff}^s = \frac{y_f y_{\alpha\beta}}{m_\phi^2} [\bar{\nu}_\alpha(p_3)\nu_\beta(p_2)] [\bar{f}(p_1)f(p_4)], \quad (2.4)$$

where,

- $\alpha, \beta = (e, \mu, \tau)$ refers to the three active ν -flavors,
- $f(\bar{f})$ represents matter fermions (anti-fermions),
- y_f is the Yukawa coupling of scalar ϕ with matter fermions f , and,
- $y_{\alpha\beta}$ is the Yukawa coupling of ϕ with the active ν -flavors.

The presence of Yukawa terms in equation 2.4 prevents us from converting it to vector currents. Consequently, it does not manifest itself as an additional matter potential. In contrast, the contribution of scalar NSI is a perturbation to the mass term in the ν -Hamiltonian. Thus, the presence of scalar NSI modifies the Dirac equation as follows.

$$\bar{\nu}_\beta \left[i\partial_\mu \gamma^\mu + \left(M_{\beta\alpha} + \frac{\sum_f n_f y_f y_{\alpha\beta}}{m_\phi^2} \right) \right] \nu_\alpha = 0, \quad (2.5)$$

where n_f represents the number density of matter fermions. The effective form of matter Hamiltonian with scalar NSI correction can be framed as,

$$\mathcal{H}_{SNSI} \equiv E_\nu + \frac{M_{eff} M_{eff}^\dagger}{2E_\nu} \pm V_{SI}. \quad (2.6)$$

In equation 2.6, the effective ν -mass matrix (M_{eff}) has contributions from the genuine ν -mass matrix (M) as well as the correction due to scalar NSI i.e. $M_{SNSI} \equiv \sum_f n_f y_f y_{\alpha\beta}/m_\phi^2$. The effective mass matrix can be expressed as $M_{eff} = M + M_{SNSI}$. The ν -mass matrix can be diagonalized by the mixing matrix \mathcal{U}' . \mathcal{U}' has the form $P\mathcal{U}Q^\dagger$, with P and Q representing an unphysical rephasing matrix and the Majorana rephasing matrix respectively. We can rotate away the Majorana rephasing matrix by $QD_\nu Q^\dagger = D_\nu$, but the diagonal rephasing matrix P can not be rotated away. Therefore, rotating the unphysical rephasing matrix P into scalar NSI correction and denoting it as δM , we have M_{eff} as,

$$M_{eff} \equiv \mathcal{U} D_\nu \mathcal{U}^\dagger + P^\dagger M_{SNSI} P \equiv M + \delta M, \quad (2.7)$$

where,

$$\delta M \equiv S_m \begin{pmatrix} \eta_{ee} & \eta_{e\mu} & \eta_{e\tau} \\ \eta_{e\mu}^* & \eta_{\mu\mu} & \eta_{\mu\tau} \\ \eta_{e\tau}^* & \eta_{\mu\tau}^* & \eta_{\tau\tau} \end{pmatrix}. \quad (2.8)$$

We use a similar parameterization of δM as shown in [111, 117, 118]. A rescaling factor of S_m is introduced in order to match the dimension with the ν -mass matrix. In this work, S_m is fixed to be $\sqrt{2.55 \times 10^{-3} eV^2}$ which corresponds to the magnitude of atmospheric mass-squared splitting $\sqrt{|\Delta m_{31}^2|}$. The factor S_m introduced is merely a rescaling of the matrix such that $\eta_{\alpha\beta}$ are dimensionless parameters that signify only the strength of scalar NSI. The hermiticity of the Hamiltonian allows the diagonal parameters to be real and the off-diagonal parameters to be complex. In this work, the effects of diagonal scalar NSI parameters are explored by taking one element at once. The forms of M_{eff} for the three cases are shown in table 1. Note that, using these forms of M_{eff} in equation 2.6, we can calculate \mathcal{H}_{SNSI} . Due to the presence of δM term, we will see a dependence on the absolute ν -mass in addition to the dependence on Δm_{ij}^2 .

An intriguing implication of scalar NSI is its dependence on the absolute ν -mass as explored in reference [28]. All the values of scalar NSI parameters $\eta_{\alpha\beta}$ are defined at matter density $\rho=2.9$ g/cc. We have scaled the $\eta_{\alpha\beta}$ values for the densities of the experiments i.e. DUNE, HK and HK+KNO. However, the impact of rescaling $\eta_{\alpha\beta}$ values is nominal for the chosen LBL experiments.

Case	Scalar NSI parameter	M_{eff}
I	η_{ee}	$\mathcal{U} \cdot D_\nu \cdot \mathcal{U}^\dagger + S_m \text{diag}(\eta_{ee}, 0, 0)$
II	$\eta_{\mu\mu}$	$\mathcal{U} \cdot D_\nu \cdot \mathcal{U}^\dagger + S_m \text{diag}(0, \eta_{\mu\mu}, 0)$
III	$\eta_{\tau\tau}$	$\mathcal{U} \cdot D_\nu \cdot \mathcal{U}^\dagger + S_m \text{diag}(0, 0, \eta_{\tau\tau})$

Table 1: Cases of M_{eff} for the diagonal scalar NSI parameters.

3 Methodology

We describe the methodology of our work here. We first give the details of the simulation of the experiments in section 3.1. We then mention the details and specifications of the three chosen LBL experiments in section 3.2.

3.1 Simulation Details

In this work, we have mainly focused on exploring the impact of diagonal scalar NSI parameters on the MO sensitivities at LBL experiments. We have used the simulation package i.e. General Long Baseline Experiment Simulator (GLOBES) [131–133] for our numerical simulations of the experiments. The values of oscillation parameters used in our analysis are listed in table 2.

Parameters	True Values	Marginalization range
θ_{12} [°]	34.51	fixed
θ_{23} [°]	47	$40 \rightarrow 50$
θ_{13} [°]	8.44	fixed
δ_{CP}	$-\pi/2$	$-\pi \rightarrow \pi$
Δm_{21}^2 [$10^{-5} eV^2$]	7.56	$6.82 \rightarrow 8.04$
Δm_{31}^2 (NO) [$10^{-3} eV^2$]	2.55	(2.25 - 2.65)
Δm_{31}^2 (IO) [$10^{-3} eV^2$]	-2.49	- (2.25 - 2.65)

Table 2: Benchmark values of ν -oscillation parameters used in GLOBES simulation [134].

In order to study the sensitivity of experiments towards the determination of neutrino MO, we define a statistical χ^2 as

$$\chi^2 \equiv \min_{\eta} \sum_i \sum_j \frac{\left[N_{true}^{i,j} - N_{test}^{i,j} \right]^2}{N_{true}^{i,j}}, \quad (3.1)$$

where, $N_{true}^{i,j}$ ($N_{test}^{i,j}$) are the number of true (test) events in the $\{i, j\}$ -th bin. The measure of statistical significance is obtained via a minimization over all the systematic uncertainties which are incorporated in the χ^2 using pull method [131, 135]. We have also incorporated the uncertainties on the oscillation parameters in the GLOBES simulation for the calculation of χ^2 . We have marginalized over the oscillation parameters θ_{23} , δ_{CP} and the mass-squared splitting in the range as shown in the third column of table 2. Throughout this work, we

have fixed the lightest neutrino mass m_1 (m_3) at 10^{-5} eV for normal (inverted) mass ordering and the other neutrino masses are calculated accordingly from the best-fit values of Δm_{21}^2 and Δm_{31}^2 respectively. However, a prior scan of probability and sensitivity with respect to the various choices of the absolute neutrino masses is shown in Appendix 5. This also accounts for the cosmological bound on the sum of neutrino masses i.e. $\sum_i m_i < 0.12$ eV [136]. In our analysis, we have considered the higher octant of θ_{23} as the true octant. In order to study the impact of scalar NSI on the MO sensitivities, we have considered three upcoming LBL experiments viz. DUNE, HK and HK+KNO. The detailed experimental setup and configuration of the detectors are discussed in the section 3.2.

3.2 Overview of the three LBL experiments

The experimental systematics and background information are taken from the Technical Design Reports (TDR) of the corresponding experiments. The details of the experiments are summarised in table 3. In the subsequent sections, we briefly discuss the technical details of the three future LBL ν -experiments viz. DUNE, HK, and HK+KNO.

3.2.1 DUNE

The Deep Underground Neutrino Experiment (DUNE) [137–141] is a flagship accelerator-based ν -experiment to be hosted by Fermilab. The Long-Baseline Neutrino Facility (LBNF) of Fermilab which can deliver 1.1×10^{21} proton on target (POT) per year with its 1.2 MW proton beam will produce the neutrinos for the experiment. It will have two detectors, the near detector at Fermilab will be situated 60m underground and will have a baseline of 574 meters. The far detector with a 1300 km baseline will be situated 1.5 km below the earth's surface at the Sanford Underground Research Facility, South Dakota. The far detector module will consist of four Liquid Argon Time Projection Chambers (LArTPC) each having a fiducial mass of 10 kt. The excellent energy reconstruction, 3D image tracking and particle identification capabilities of LArTPC technology will provide exceptional precision to DUNE in probing neutrino properties.

3.2.2 HK

In our analysis, we have referred the Tokai to Hyper-Kamiokande (T2HK) [87] detector as HK. This will be a long-baseline counterpart of the Hyper-Kamiokande (Hyper-K) experiment which is an upgradation of the successful Super-Kamiokande (Super-K) experiment. It will have a water Cherenkov (WC) detector of fiducial mass of 187 kt which will be 8.4 times larger than its predecessor Super-K. It will use neutrinos produced by the 1.2 MW beam at the J-PARC beam facility in Japan. It can produce 27×10^{21} POT per year. The neutrinos will be detected by the Hyper-K detector situated 2.5° off-axis from the beam facility at the baseline of 295 km.

3.2.3 HK+KNO

Tokai to Hyper-Kamiokande to Korea [88] a.k.a. T2HKK is referred to as HK+KNO in our analysis. Korean Neutrino Observatory (KNO) is the second water Cherenkov detector which is planned to be placed at Korea at a distance of 1100 km from the J-PARC facility.

Experiment details	Channels	Normalization error	
		Signal	Background
DUNE Baseline = 1300 km L/E = 1543 km/GeV Fiducial mass = 40 kt (LArTPC) Runtime = 3.5 yr ν + 3.5 yr $\bar{\nu}$	$\nu_e(\bar{\nu}_e)$ appearance $\nu_\mu(\bar{\nu}_\mu)$ disappearance	2 % (2%) 5 % (5 %)	5 % (5 %) 5 % (5 %)
HK Baseline = 295 km L/E = 527 km/GeV Fiducial mass = 187 kt (WC) Runtime = 2.5 yr ν + 7.5 yr $\bar{\nu}$	$\nu_e(\bar{\nu}_e)$ appearance $\nu_\mu(\bar{\nu}_\mu)$ disappearance	3.2 % (3.9 %) 3.6 % (3.6 %)	10 % (10 %) 10 % (10 %)
HK+KNO Baseline = 295, 1100km L/E = 527, 1964 km/GeV Fiducial mass = 187, 187 kt(WC) Runtime = 2.5 yr ν + 7.5 yr $\bar{\nu}$	$\nu_e(\bar{\nu}_e)$ appearance $\nu_\mu(\bar{\nu}_\mu)$ disappearance	3.2 % (3.9 %) 3.6 % (3.6 %)	10 % (10 %) 10 % (10 %)

Table 3: Detector details and systematic uncertainties for DUNE, HK and HK+KNO.

It is an extension of Hyper-K experiment which will consist of two WC detectors, one 187 kt detector at a baseline of 295 km in Japan (HK), and another identical detector with a baseline of 1100 km in Korea (KNO). The 2.5° off-axis beam at a baseline of HK+KNO will enable us to study the oscillations at second oscillations maxima at an energy $\sim 0.6\text{eV}$.

4 Results and Discussion

We discuss the impact of diagonal scalar NSI elements ($\eta_{ee}, \eta_{\mu\mu}, \eta_{\tau\tau}$) on the appearance ν -oscillation probability ($P_{\mu e}$), for NO and IO, and how it affects the MO sensitivities in LBL experiments (DUNE, HK, HK+KNO). The presence of scalar NSI leads to a correction in the ν -mass matrix which can modify values of $P_{\mu e}$. In section 4.1, we first explore the impact of diagonal scalar NSI parameters on $P_{\mu e}$ for varied neutrino energies. We also study its effects on the MO-asymmetry parameter to further investigate its impact on MO determination at the probability level in section 4.2. The impact of scalar NSI on the MO sensitivities is presented in section 4.3. The MO sensitivities for the synergy of DUNE with HK and HK+KNO in the presence of scalar NSI are shown in section 4.4. In section 4.5, we explore the Δm_{31}^2 constraining capability of the experiments in presence of scalar NSI.

4.1 Effects on the appearance channel $P_{\mu e}$

The impact of diagonal scalar NSI elements ($\eta_{ee}, \eta_{\mu\mu}, \eta_{\tau\tau}$) on $P_{\mu e}$ for varying neutrino energy (E) at baselines corresponding to DUNE, HK and HK+KNO are shown in figure 1, 2 and 3 respectively. We observe that,

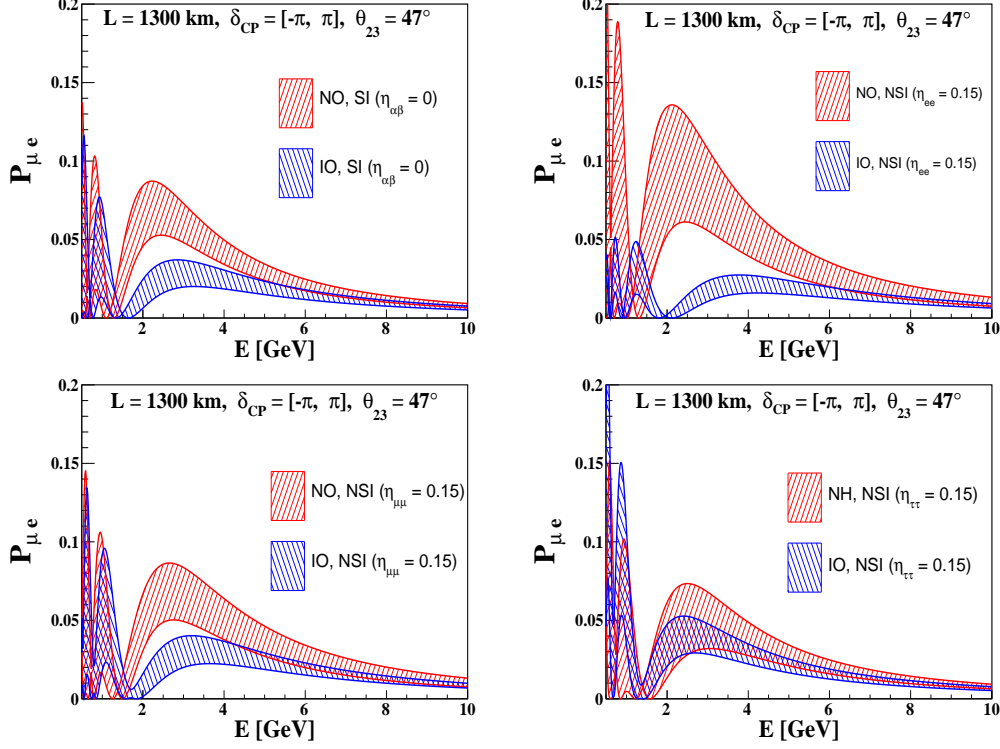


Figure 1: $P_{\mu e}$ vs E at the DUNE-baseline of 1300km in the presence of scalar NSI, for NO (red band) and IO (blue band). Both the bands correspond to δ_{CP} values $\in [-\pi, \pi]$. The panels correspond to no scalar NSI (top-left), η_{ee} (top-right), $\eta_{\mu\mu}$ (bottom-left) and $\eta_{\tau\tau}$ (bottom-right).

- For no scalar NSI case, the DUNE baseline can clearly distinguish between the NO and IO in the energy range $\sim [1.5, 4]$ GeV. The presence of η_{ee} widens the energy range as well as the separation between the mass orderings. The $\eta_{\mu\mu}$ element marginally reduces the separation between the mass orderings and the energy window of the ordering separation. For $\eta_{\tau\tau}$ element, a significant overlapping of bands can be seen.
- For HK baseline, we observe an overlap between the NO and IO bands for the no scalar NSI case. The presence of η_{ee} leads to a larger separation between the bands in the energy range $\sim [0.4, 0.7]$ GeV. For instance, if η_{ee} is known to be exactly 0.15 from other experiments, a larger separation between the two bands would indicate a better measurement of the mass ordering. The chosen value of the element $\eta_{\mu\mu}$ shows a nominal change compared to the no scalar NSI case. For $\eta_{\tau\tau}$, the IO band lies above the NO band without any distinct separation between the mass orderings.
- For HK+KNO baseline, we observe clear discrimination between the mass orderings at the probability level in the energy window $\sim [1.5, 3]$ GeV in the absence of scalar NSI. The presence of η_{ee} element widens the band separation as well as the energy window. The element $\eta_{\mu\mu}$ reduces both the amplitude as well as the discriminating

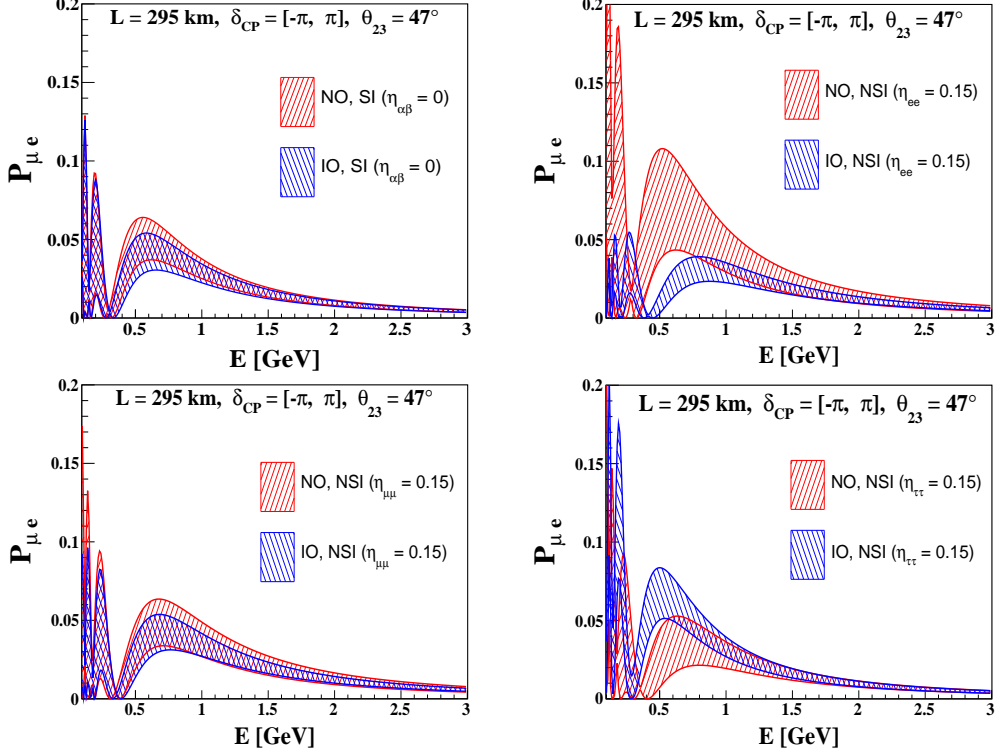


Figure 2: $P_{\mu e}$ vs E at the HK-baseline of 295km in the presence of scalar NSI, for NO (red band) and IO (blue band). Both the bands correspond to δ_{CP} values $\in [-\pi, \pi]$. The panels correspond to no scalar NSI (top-left), η_{ee} (top-right), $\eta_{\mu\mu}$ (bottom-left) and $\eta_{\tau\tau}$ (bottom-right).

power of the neutrino MO. For $\eta_{\tau\tau}$, both the NO and IO band are seen to completely overlap.

We have also further explored the impact of scalar NSI as a function of $\Delta P_{\mu e}(= P_{\mu e}^{NSI} - P_{\mu e}^{SI})$ in the Δm_{31}^2 - E parameter space for all the three experiments which are shown in appendix 5.

4.2 Imprints on the MO asymmetry

In order to quantify the effects of scalar NSI on the MO determination at the probability level, we define an mass ordering asymmetry parameter as

$$A_{MO} = \frac{P_{\mu e}^{NO} - P_{\mu e}^{IO}}{P_{\mu e}^{NO} + P_{\mu e}^{IO}}, \quad (4.1)$$

where, $P_{\mu e}^{NO}$ and $P_{\mu e}^{IO}$ are the appearance probabilities for NO and IO respectively. This asymmetry parameter may quantify an experiment's capability towards discriminating between the two ν -mass orderings.

In figure 4, we show the deviation of A_{MO} as a function of δ_{CP} for the baselines of DUNE (left-panel), HK (middle-panel) and HK+KNO (right-panel) respectively. We have

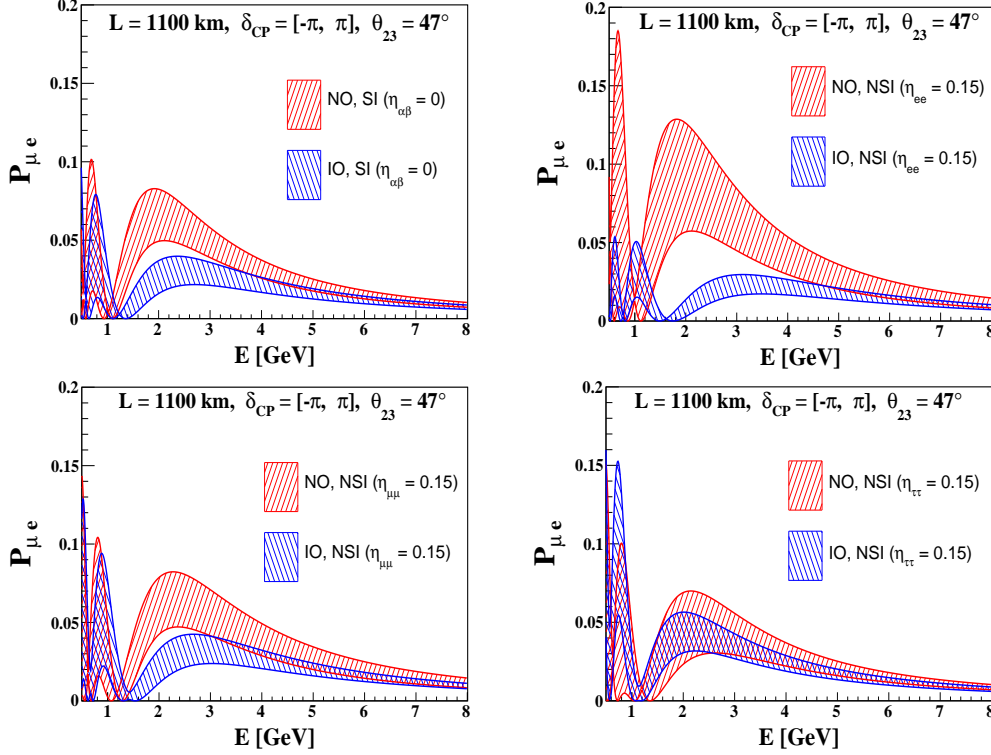


Figure 3: $P_{\mu e}$ vs E at the HK+KNO-baseline of 1100km in the presence of scalar NSI, for NO (red band) and IO (blue band). Both the bands correspond to δ_{CP} values $\in [-\pi, \pi]$. The panels correspond to no scalar NSI (top-left), η_{ee} (top-right), $\eta_{\mu\mu}$ (bottom-left) and $\eta_{\tau\tau}$ (bottom-right).

chosen the neutrino energies as their respective peak energies i.e. 2.5 GeV (DUNE), 0.6 GeV (HK) and 0.66 GeV (HK+KNO). We note the following.

- At DUNE, the presence of positive (negative) η_{ee} can enhance (suppress) A_{MO} as compared to no scalar NSI case. The effect of $\eta_{\mu\mu}$ is nominal on A_{MO} . A positive value of the $\eta_{\tau\tau}$ suppresses A_{MO} , while a negative $\eta_{\tau\tau}$ nominally enhances A_{MO} .
- For no scalar NSI, HK has nominal sensitivity towards the neutrino MO as compared to DUNE. The presence of positive (negative) η_{ee} can enhance (suppress) A_{MO} . The $\eta_{\mu\mu}$ element shows a similar effect on A_{MO} as compared to no scalar NSI case. However, a negative (positive) $\eta_{\tau\tau}$ enhances (suppresses) A_{MO} .
- For HK+KNO, we see a suppression in A_{MO} for positive values of $\eta_{\tau\tau}$ in the range $\delta_{CP} \sim [40^\circ, 180^\circ]$. A negative η_{ee} , mostly suppresses A_{MO} except in the range $\delta_{CP} \sim [0^\circ, 90^\circ]$. A negative $\eta_{\mu\mu}$ mostly suppresses A_{MO} , while a positive $\eta_{\mu\mu}$ enhances A_{MO} in the range $\delta_{CP} \sim [-70^\circ, 60^\circ]$. The positive $\eta_{\tau\tau}$ reduces the experiment's sensitivity towards MO for the complete δ_{CP} parameter space.

We observe that the presence of diagonal scalar NSI elements leads to a significant modification in the values of $P_{\mu e}$. As a result, it can substantially enhance/hamper the MO

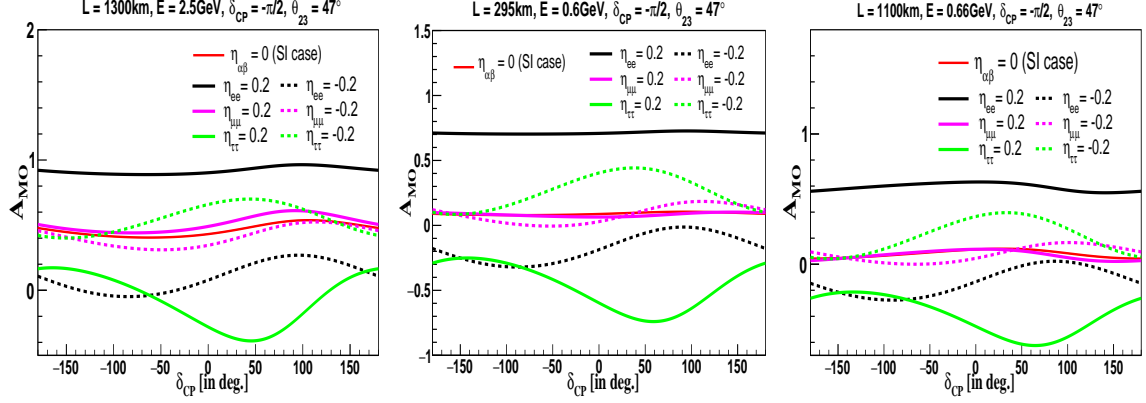


Figure 4: Impact of scalar NSI on A_{MO} at DUNE (left-panel), HK (middle-panel) and HK+KNO (right-panel) baselines. The red solid line corresponds to no scalar NSI case. The solid (dashed) lines correspond to positive (negative) diagonal scalar NSI parameters as indicated in the legends.

sensitivities of these LBL experiments.

4.3 Impact on the MO sensitivities

One of the major goals of the current and upcoming LBL ν -oscillation experiments is the determination of neutrino mass ordering. The impact of scalar NSI on the MO sensitivities at three different LBL experiments i.e. DUNE, HK and HK+KNO is explored here. We have considered two different cases in our analysis i.e.,

- Considering NO as the true mass ordering for which $\Delta\chi^2$ can be defined as,

$$\Delta\chi_{MO}^2 = \chi_{NO}^2 - \chi_{IO}^2 \quad (\text{for true NO}). \quad (4.2)$$

- Considering IO as the true mass ordering for which $\Delta\chi^2$ can be defined as,

$$\Delta\chi_{MO}^2 = \chi_{IO}^2 - \chi_{NO}^2 \quad (\text{for true IO}). \quad (4.3)$$

To obtain the MO sensitivities, the statistical significance which is defined as $\sigma = \sqrt{\Delta\chi^2}$ is plotted for varying true δ_{CP} in $[-\pi, \pi]$. The other ν -oscillation parameters are fixed at values as listed in table 2. In figure 5-9, we have marginalized over the test ordering as well as δ_{CP} in $[-\pi, \pi]$ and θ_{23} in $[40^\circ, 50^\circ]$. We have also additionally marginalized over the scalar NSI parameters in the range $[-0.2, 0.2]$.

In figure 5, we show the effects of scalar NSI on the MO sensitivity of DUNE considering NO (IO) as the true ordering in the top-panel (bottom-panel). The solid red line corresponds to the case with no scalar NSI effects. The solid (dashed) lines correspond to the positive (negative) values of scalar NSI parameters. The dashed magenta and green lines represent the 5σ and 3σ CL respectively. We observe that,

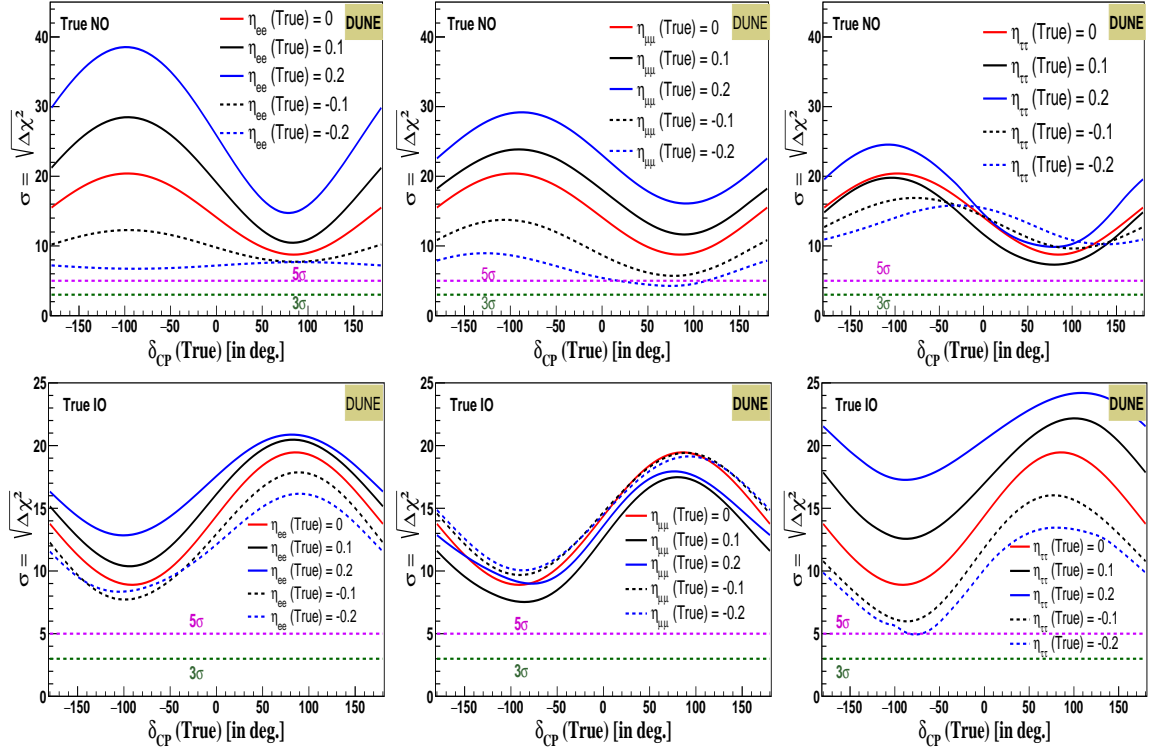


Figure 5: The MO sensitivity of DUNE, in the presence of scalar NSI, for true NO (top-panel) and true IO (bottom-panel). The effects of diagonal scalar NSI parameters η_{ee} , $\eta_{\mu\mu}$ and $\eta_{\tau\tau}$ are shown in left, middle and right panels respectively. The solid red line is for no-scalar NSI case. The solid (dashed) lines are for non-zero positive (negative) scalar NSI parameters.

- For true NO, positive (negative) values of η_{ee} and $\eta_{\mu\mu}$ elements enhance (suppress) the MO sensitivities as compared to no scalar NSI case. For $\eta_{\tau\tau} = 0.2$, the sensitivities show an enhancement for most values of δ_{CP} , while for $\eta_{\tau\tau} = 0.1$, the sensitivities lie below the no scalar NSI case for the whole δ_{CP} parameter space. For the chosen negative values of $\eta_{\tau\tau}$, the sensitivities lie mostly below the no scalar NSI case.
- For true IO, positive (negative) values of η_{ee} and $\eta_{\tau\tau}$, enhance (suppress) the MO sensitivities as compared to when there is no scalar NSI present. However, for a positive (negative) $\eta_{\mu\mu}$ value the sensitivities get mostly suppressed (enhanced).

In figure 6, we present the MO sensitivities of HK in presence of scalar NSI parameters η_{ee} (left-panel), $\eta_{\mu\mu}$ (middle-panel) and $\eta_{\tau\tau}$ (right-panel) assuming NO (IO) as true ordering in the top-panel (bottom-panel). The no scalar NSI case is depicted by the red line, whereas the positive (negative) scalar NSI parameters are shown by the solid (dashed) lines. The 5σ (3σ) CL are represented by the horizontal magenta (green) lines. The observations made are listed below.

- For true NO, a positive value of the $\eta_{\alpha\beta}$ mostly enhances the sensitivity towards MO

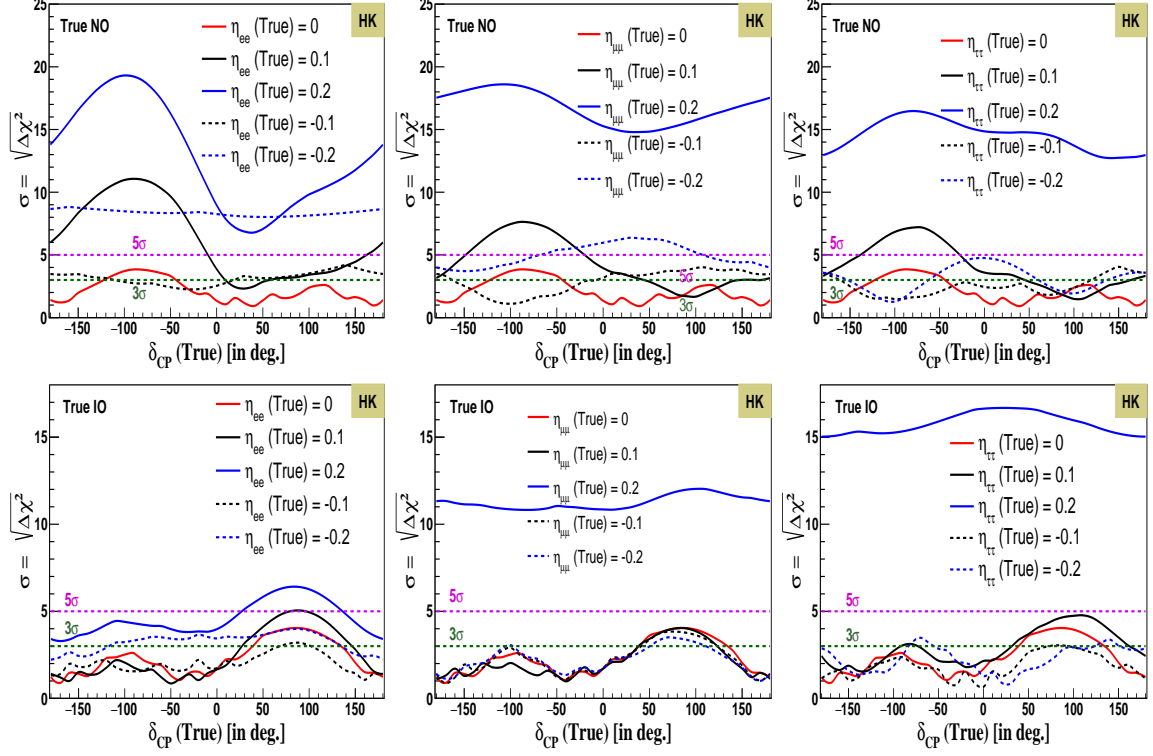


Figure 6: The MO sensitivity of HK, in the presence of scalar NSI, for true NO (top-panel) and true IO (bottom-panel). The effects of diagonal scalar NSI parameters η_{ee} , $\eta_{\mu\mu}$ and $\eta_{\tau\tau}$ are shown in left, middle and right panels respectively. The solid red line is for no-scalar NSI case. The solid (dashed) lines are for non-zero positive (negative) scalar NSI parameters.

determination. Even with $\eta_{\alpha\beta} = 0.1$, above 5σ sensitivity is observed in the negative half-plane of δ_{CP} . For most values of δ_{CP} , negative values of scalar NSI parameters also enhance the sensitivities as compared to no scalar NSI case. A suppression in the sensitivity can be observed for some combinations of δ_{CP} and negative $\eta_{\alpha\beta}$.

- For true IO, a significant enhancement in the ordering sensitivity is observed only for $\eta_{\alpha\beta} = 0.2$, particularly for $\eta_{\mu\mu}$ and $\eta_{\tau\tau}$. For $\eta_{\mu\mu} = 0.1$, the sensitivity curves with and without scalar NSI cases are seen to nearly overlap for the entire range of δ_{CP} values.

In figure 7, we have shown the effects of diagonal scalar NSI parameters on the MO sensitivities at HK+KNO. The top (bottom) panel corresponds to MO sensitivity for true NO (IO) with non-zero η_{ee} (left-panel), $\eta_{\mu\mu}$ (middle-panel) and $\eta_{\tau\tau}$ (right-panel). The red solid line is in the absence of scalar NSI, whereas, the black and blue lines correspond to non-zero scalar NSI parameters. The solid (dashed) lines correspond to positive (negative) values of scalar NSI parameters. The 5σ (dashed magenta) and 3σ (dashed green) CL are drawn as a reference. The following are the observations from figure 7.

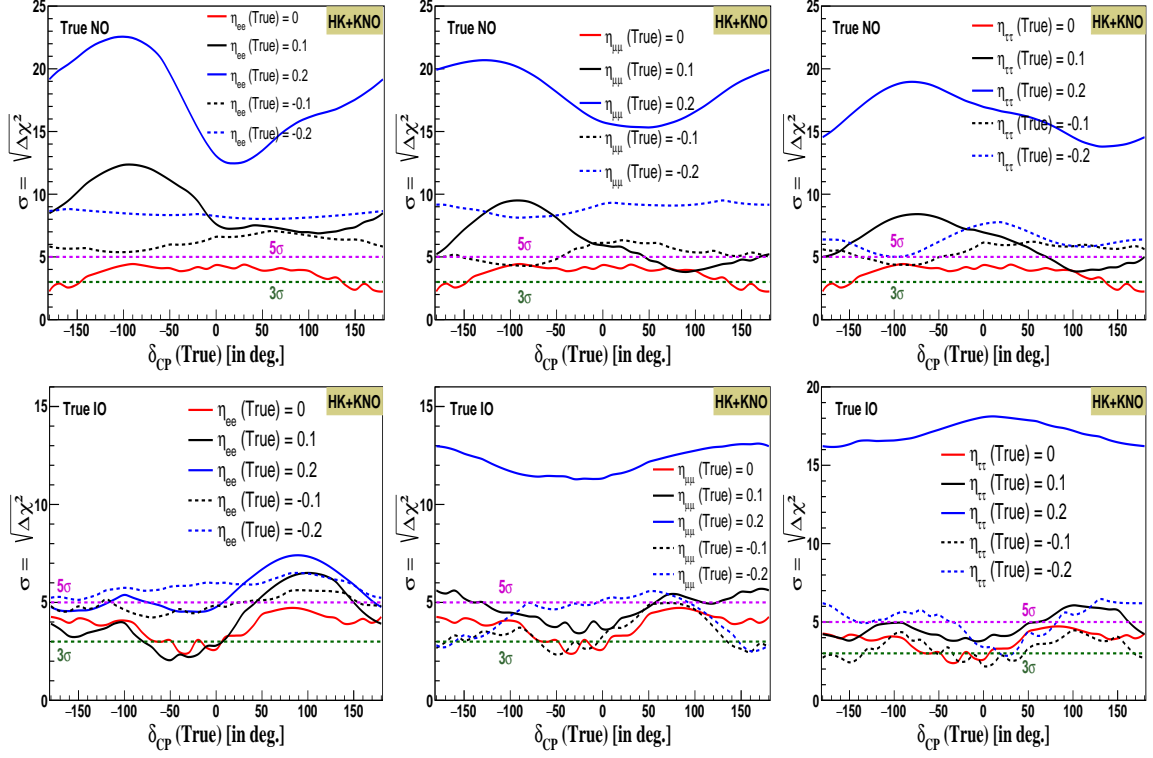


Figure 7: The MO sensitivity of HK+KNO, in the presence of scalar NSI, for true NO (top-panel) and true IO (bottom-panel). The effects of diagonal scalar NSI parameters η_{ee} , $\eta_{\mu\mu}$ and $\eta_{\tau\tau}$ are shown in left, middle and right panels respectively. The solid red line is for no-scalar NSI case. The solid (dashed) lines are for non-zero positive (negative) scalar NSI parameters.

- For NO as the true ordering, the sensitivity is enhanced for both positive and negative values of scalar NSI parameters. In general, with scalar NSI we get above 5σ MO sensitivity except for the case when $\eta_{\mu\mu}$ and $\eta_{\tau\tau}$ has the value of -0.1 and δ_{CP} falls within the range of $[-120^\circ, -60^\circ]$.
- For IO as the true ordering, a substantial enhancement in sensitivity is observed only when $\eta_{\mu\mu}$ and $\eta_{\tau\tau}$ is equal to 0.2 . The effect of scalar NSI, for all other cases, is nominal. Although, certain values of η_{ee} can improve the sensitivity beyond 5σ for some range of δ_{CP} .

4.4 The MO sensitivity for the Synergy of the LBL experiments

We here show the effects of scalar NSI on the MO sensitivities after combining the data from two LBL experiments viz. DUNE+HK (in section 4.4.1) and DUNE+HK+KNO (in section 4.4.2) respectively.

4.4.1 Combining DUNE with HK

In figure 8, the neutrino MO sensitivity of the combination of DUNE and HK in the presence of scalar NSI is shown. The top panel represents the true NO, whereas the bottom panel represents the true IO case. The non-zero positive (negative) values of diagonal scalar NSI parameters are depicted by the blue and black solid (dashed) curves. The red solid curve corresponds to the no scalar NSI case, with 5σ and 3σ CL represented by dashed magenta and green lines respectively. The observations from figure 8 are,

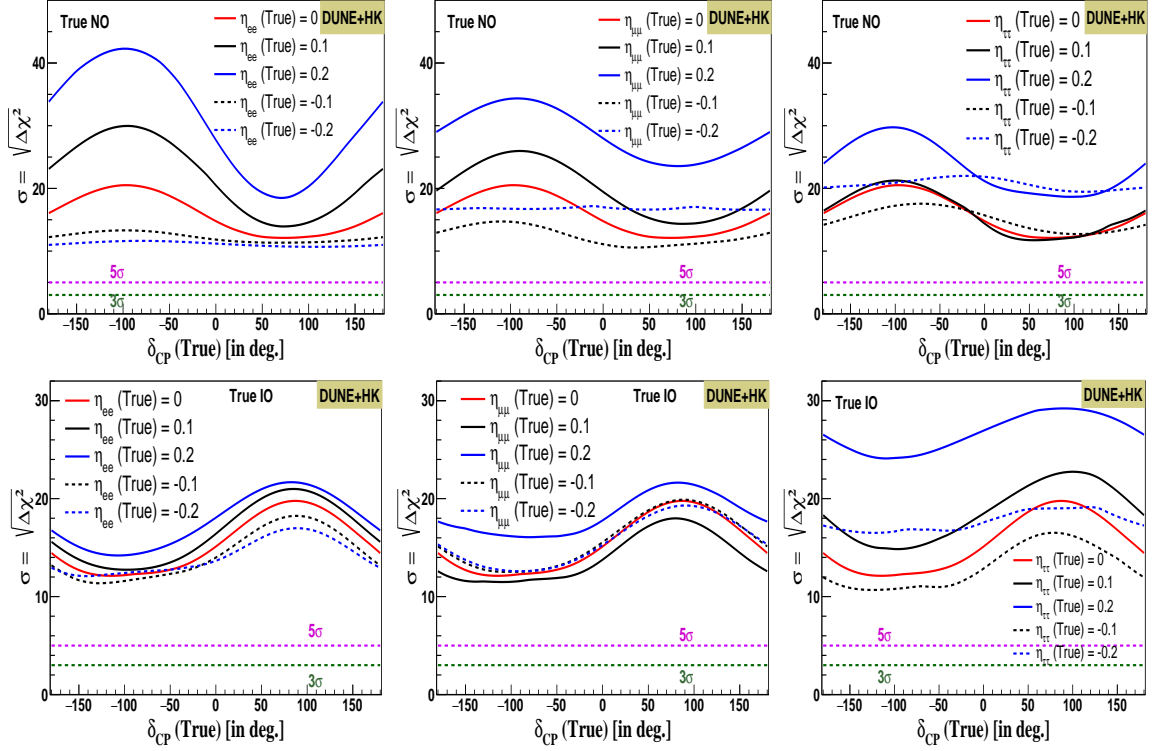


Figure 8: The impact of diagonal scalar NSI parameters on the MO sensitivities for DUNE+HK for true NO (top-panel) and IO (bottom-panel) in the presence of diagonal scalar NSI parameters: η_{ee} (left-panel), $\eta_{\mu\mu}$ (middle-panel) and $\eta_{\tau\tau}$ (right-panel). The solid red line is for no-scalar NSI case. The solid (dashed) lines are for non-zero positive (negative) scalar NSI parameters.

- In case of DUNE+HK, the MO sensitivity is above 5σ CL for all values of δ_{CP} . In the presence of scalar NSI, for the true NO case, positive (negative) η_{ee} and $\eta_{\mu\mu}$ mostly improve (deteriorate) the MO sensitivity. However, for $\eta_{\mu\mu}$ and $\eta_{\tau\tau}$ fixed at -0.2, an enhancement in the sensitivity towards MO determination can be seen.
- For IO as true ordering, the positive (negative) η_{ee} and $\eta_{\tau\tau}$ enhances (suppresses) the MO sensitivity for DUNE+HK. The effect is more prominent for $\eta_{\tau\tau}$ as compared to η_{ee} . Although for $\eta_{\tau\tau} = -0.2$, the MO sensitivity is enhanced for most values of δ_{CP} . For $\eta_{\mu\mu} = 0.2$, the sensitivity is enhanced, whereas $\eta_{\mu\mu} = 0.1$ suppresses the MO

sensitivity. In the case of negative $\eta_{\mu\mu}$, the sensitivity curves largely overlap with the no scalar NSI case across various values of δ_{CP} .

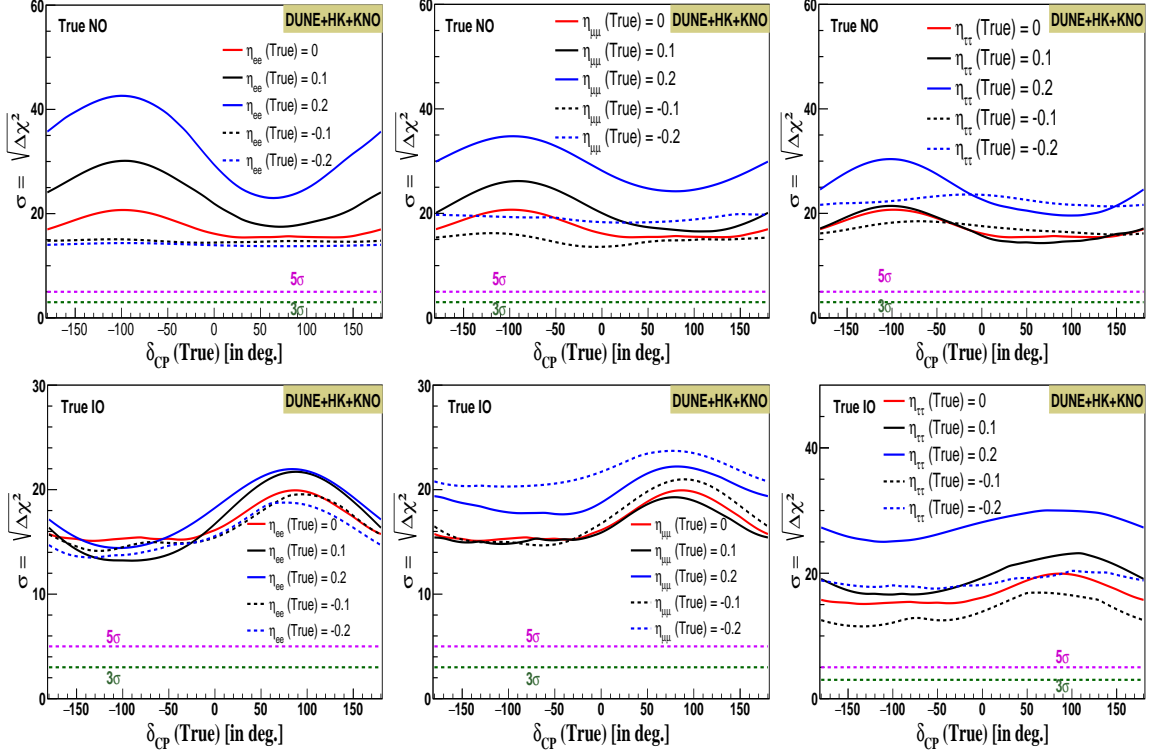


Figure 9: The impact of scalar NSI on MO sensitivities for DUNE+HK+KNO in the presence of diagonal scalar NSI parameters: η_{ee} (left-panel), $\eta_{\mu\mu}$ (middle-panel) and $\eta_{\tau\tau}$ (right-panel). The top-panel corresponds to true NO and the bottom-panel corresponds to true IO. The solid red line is for no-scalar NSI case. The solid (dashed) lines are for non-zero positive (negative) scalar NSI parameters.

4.4.2 Combining DUNE with HK+KNO

The MO sensitivity of DUNE+HK+KNO for true NO (top-panel) and true IO (bottom-panel) is shown in figure 9. The red solid line represents the case without scalar NSI and other coloured lines represent non-zero values of η_{ee} (left-panel), $\eta_{\mu\mu}$ (middle-panel) and $\eta_{\tau\tau}$ (right-panel) as indicated in the legends. The 5σ and 3σ CL are drawn in magenta and green colours. We observe that,

- For true NO, a positive (negative) η_{ee} and $\eta_{\mu\mu}$ enhances (suppresses) the MO sensitivities for most values of δ_{CP} except for $\eta_{\mu\mu} = -0.2$. For $\eta_{\tau\tau} = \pm 0.2$, MO sensitivities are enhanced whereas $\eta_{\tau\tau} = 0.1$ mostly overlaps with the standard MO sensitivities and $\eta_{\tau\tau} = -0.1$ suppresses in the region of $\delta_{CP} \in [-40^\circ, -180^\circ]$.
- For true IO, the effect of $\eta_{\tau\tau}$ is prominent as compared to η_{ee} and $\eta_{\mu\mu}$. The positive values of $\eta_{\alpha\beta}$ enhances the sensitivities except for η_{ee} in the negative δ_{CP} -plane. A

negative value of η_{ee} mostly suppresses the MO sensitivities. For negative $\eta_{\mu\mu}$, we see an enhancement in the MO sensitivities. For $\eta_{\tau\tau}$ fixed at -0.2 (-0.1), the MO sensitivities are enhanced (suppressed) for the complete δ_{CP} space.

- In both the scenarios of true NO and true IO, we observe a similar trend to those of the DUNE+HK configuration. This similarity is expected since the detectors used in both setups are identical. However, in the case of DUNE+HK+KNO, the effects are more prominent due to its longer baseline, as scalar NSI varies linearly with the environmental matter density.

4.5 Precision measurement of Δm_{31}^2

We look into the impact of diagonal scalar NSI elements η_{ee} , $\eta_{\mu\mu}$ and $\eta_{\tau\tau}$ on the precision measurements of Δm_{31}^2 at DUNE, HK and HK+KNO. We have also performed combined analyses for DUNE+HK and DUNE+HK+KNO. We present the results in figure 10. The magenta and green dashed lines represent the 5σ and 3σ CL respectively. The red solid line represents the DUNE case. In the top (bottom) panel, the black and blue solid lines represent the case HK (HK+KNO) and DUNE+HK (DUNE+HK+KNO) respectively. We have considered the higher θ_{23} octant as the true octant and NO as the true mass ordering. The true value of Δm_{31}^2 is fixed at $2.55 \times 10^{-3} eV^2$ and the test value is varied in $[2.46, 2.59] \times 10^{-3} eV^2$. We have additionally marginalized over δ_{CP} , θ_{23} and $\eta_{\alpha\beta}$. The true value of $\eta_{\alpha\beta}$ is fixed at 0.1 for all the experimental configurations. The findings obtained are stated below.

- The constraining capability of Δm_{31}^2 for DUNE+HK and DUNE+HK+KNO configuration is better compared to DUNE, HK and HK+KNO for all the cases of scalar NSI parameters. The synergies of experiments lead to a better constraining of Δm_{31}^2 in each case.
- In presence of η_{ee} and $\eta_{\tau\tau}$, the constraining of Δm_{31}^2 is nominally better in comparison to $\eta_{\mu\mu}$. This can be seen for both the synergy cases i.e. DUNE+HK and DUNE+HK+KNO.

To quantify the precision measurement of Δm_{31}^2 , we can define a quantity \mathbb{P} as,

$$\mathbb{P} = \frac{p_{max} - p_{min}}{p_{max} + p_{min}}, \quad (4.4)$$

where, p_{max} and p_{min} are the maximum value and minimum value of Δm_{31}^2 respectively, at a fixed CL. For example, if η_{ee} is determined elsewhere to be 0.1, DUNE will be able to measure Δm_{31}^2 at a precision of $\sim 1.17\%$ at 3σ CL, whereas, HK will be able to measure at a precision of $\sim 0.78\%$. HK+KNO is expected to measure the same at a precision of $\sim 0.6\%$. The synergy between DUNE and HK may significantly improve the precision to $\sim 0.58\%$. In addition, the synergy with DUNE, HK and KNO may further improve it to $\sim 0.5\%$. In presence of $\eta_{\mu\mu}$, DUNE, HK and HK+KNO will be able to measure at a precision of $\sim 1.27\%$, $\sim 0.98\%$ and $\sim 0.78\%$ respectively at 3σ CL.. A synergy of DUNE and HK

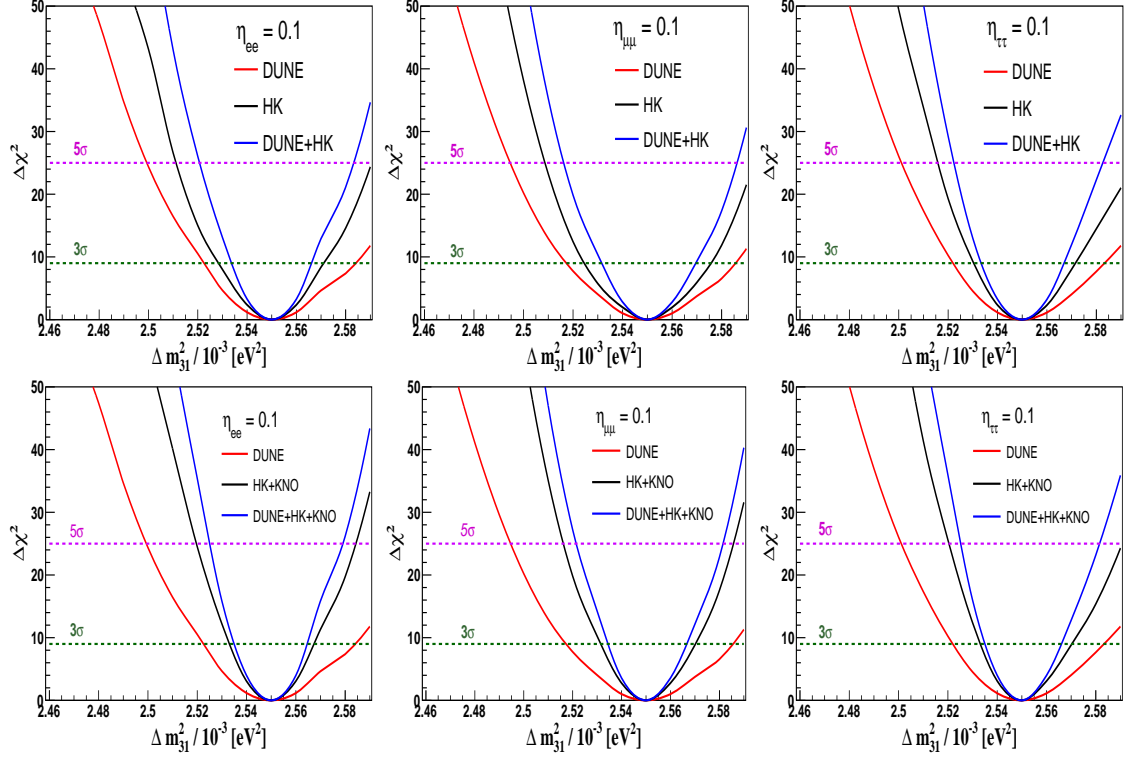


Figure 10: The impact of scalar NSI on Δm_{31}^2 constraining capability in the presence of diagonal scalar NSI parameters η_{ee} (left-panel), $\eta_{\mu\mu}$ (middle-panel) and $\eta_{\tau\tau}$ (right-panel) for true NO. The top-panel corresponds to DUNE (red), HK (black) and the combined analysis of DUNE+HK (blue), whereas the bottom-panel corresponds to DUNE (red), HK+KNO (black) and DUNE+HK+KNO (blue).

(HK+KNO) improves the number to $\sim 0.68\%$ ($\sim 0.58\%$). Similarly, in presence of $\eta_{\tau\tau}$, DUNE, HK and HK+KNO will be able to measure at a precision of $\sim 1.17\%$, $\sim 0.78\%$ and $\sim 0.68\%$ respectively at 3σ CL. And a synergy of DUNE+HK and DUNE+HK+KNO may improve the precision to $\sim 0.58\%$.

5 Summary and concluding remarks

The upcoming ν -oscillation experiments are centred on achieving precise measurements of ν -mixing parameters and addressing the unknowns in the field of neutrino physics like the determination of neutrino MO, octant of θ_{23} and the leptonic CP phase. The determination of the true neutrino MO is crucial as it holds the potential to significantly enhance our understanding of the fundamental nature of neutrinos. The existence of NSIs of neutrinos has the potential to influence the physics sensitivities of these LBL ν -experiments. The potential scalar coupling of neutrinos is one such non-standard physics scenario which may affect the neutrino MO sensitivities. Scalar NSIs of neutrinos bring a direct contribution to the ν -mass matrix which is sub-dominant in nature.

In this work, we have explored the effects of diagonal scalar NSI parameters ($\eta_{ee}, \eta_{\mu\mu}, \eta_{\tau\tau}$) on the neutrino MO sensitivities at three upcoming LBL experiments i.e. DUNE, HK and HK+KNO. We have first explored the impact of scalar NSI at the probability level for both the neutrino MO, where if the value of $\eta_{\alpha\beta}$ is exactly known from other experiments, a larger separation between the two probability bands would indicate a better measurement of the MO. We observe that the discrimination between the mass orderings is enhanced in the presence of η_{ee} for all the chosen experiments. We then explored the MO sensitivities for the individual experiments in the presence of diagonal scalar NSI parameters. We further probed the potential improvement due to the two synergy cases i.e. DUNE+HK and DUNE+HK+KNO. We have mainly focused on the impact of the presence of scalar coupling of neutrinos on the MO sensitivities. We observe that the presence of scalar NSI can significantly alter the ν -oscillation probabilities which in turn affects the sensitivities of LBL experiments towards MO determination. In MO sensitivity studies, we mostly observed an enhancement in the sensitivities for different choices of positive $\eta_{\alpha\beta}$ parameters considering true NO. However, for negative values of scalar NSI parameters, we observed suppression/enhancement depending on the combination of $\eta_{\alpha\beta}$ and δ_{CP} values. For true IO, we observe a significant overlapping of sensitivities for the standard case with the scalar NSI case for negative $\eta_{\alpha\beta}$. However, the combined analysis of DUNE+HK and/or DUNE+HK+KNO can remove the overlapping for $\eta_{\tau\tau}$ parameter due to the increased statistics over an enhanced parameter region. In presence of scalar NSI, we observe that HK and HK+KNO show better constraining capability of Δm_{31}^2 in comparison to DUNE. The combined analyses for DUNE+HK and DUNE+HK+KNO can enhance the overall constraining capability for all non-zero scalar NSI parameters.

The neutrino mass ordering stands as one of the fundamental mysteries in particle physics, the determination of which would mark a significant breakthrough in our understanding of the universe. Therefore, understanding the impact of subdominant effects arising from scalar NSIs on the MO sensitivities of LBL experiments is imperative. It is also crucial to impose constraints on the scalar NSI parameters to ensure accurate interpretation of experimental data.

Acknowledgments

The authors acknowledge the DST SERB grant CRG/2021/002961. AS would also acknowledge the fellowship received from CSIR-HRDG (09/0796(12409)/2021-EMR-I). AM thanks the support of the Research and Innovation Grant 2021 (DoRD/RIG/10-73/ 1592-A) funded by Tezpur University. DB acknowledges DST for the financial support provided through the INSPIRE fellowship.

A Scalar NSI features involving probability and sensitivity

A.1 Dependence of oscillation probabilities on ν -mass

As scalar NSI contributes directly to the neutrino mass matrix in the effective Hamiltonian. The ν -oscillation probabilities will depend not only on the mass-squared differences but

also on the absolute neutrino masses. We have explored the impact of various choices of m_{lightest} on the ν -oscillation probabilities. In figure 11, the $P_{\mu e}$ vs Energy for such neutrino mass choices are shown for both of the mass orderings at DUNE baseline. The choices of the values of the lightest neutrino mass are such that the sum of neutrino masses follows the cosmological bound i.e. $\sum m_i < 0.12$ eV. The other oscillation parameters are fixed at values as mentioned in table 2. For both mass orderings, we observe that an increase in m_{lightest} nominally suppresses $P_{\mu e}$.

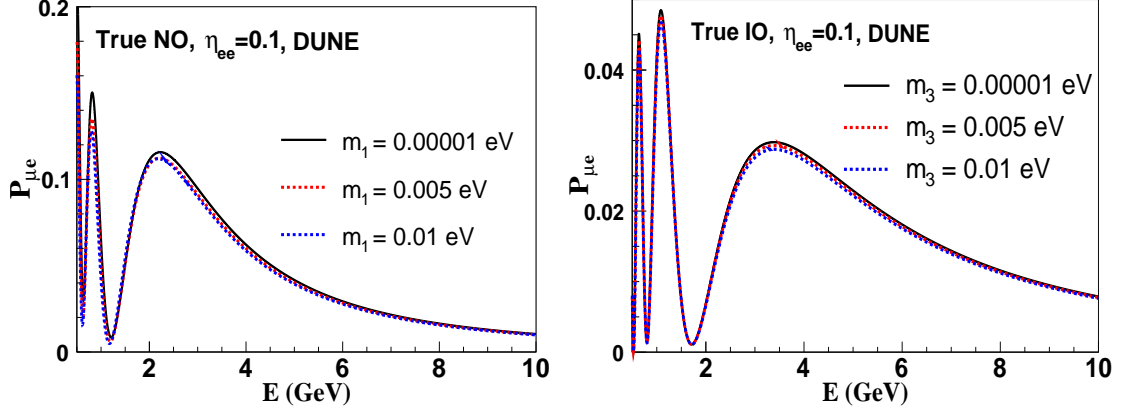


Figure 11: Impact of different choices of lightest ν -mass on $P_{\mu e}$ for the baseline of DUNE in presence of scalar NSI parameter η_{ee} fixed at 0.1. The left panel represents true NO and the right panel represents true IO.

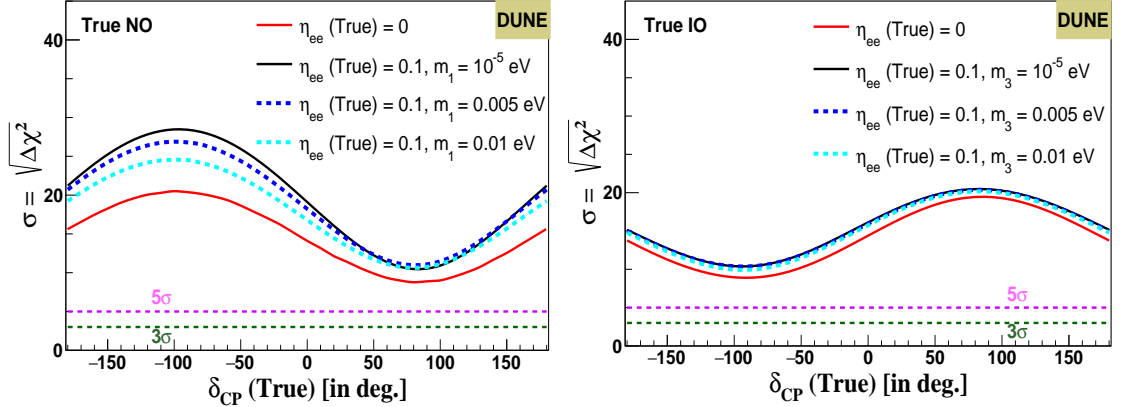


Figure 12: Impact of different choices of lightest ν -mass on the MO sensitivity at DUNE in the presence of scalar NSI parameter η_{ee} fixed at 0.1. The left (right) panel represents the true NO (IO) case. The red solid line represents the SI case. The solid black, dashed blue and dashed cyan line represents the sensitivity in the presence of η_{ee} with the lightest ν -mass fixed at 10^{-5} , 0.005 and 0.01 eV respectively.

In figure 12, the impact of the choices of m_{lightest} on the MO sensitivity of DUNE is shown. The red solid line represents the SI case. The solid black, dashed blue and dashed cyan lines represent the sensitivity in the presence of η_{ee} with the lightest ν -mass fixed at

10^{-5} , 0.005 and 0.01 eV respectively. For both of the mass orderings, the overall trend of the MO sensitivity curve remains similar. For NO, the impact of ν -mass is relatively nominal in the positive δ_{CP} -plane, whereas, a suppression with increasing ν -mass is observed in the negative δ_{CP} -plane. For IO, the MO sensitivity is marginally affected by different choices of lightest ν -mass.

A.2 Variation of $\Delta P_{\mu e}$ in Δm_{31}^2 -E parameter space

In order to quantify the impact of scalar NSI, we define a quantity $\Delta P_{\mu e}$ as

$$\Delta P_{\mu e} = P_{\mu e}^{NSI} - P_{\mu e}^{SI}$$

where, $P_{\mu e}^{NSI}$ and $P_{\mu e}^{SI}$ represents the appearance probabilities in the presence of scalar NSI and no scalar NSI cases respectively. We have plotted $\Delta P_{\mu e}$ for varying neutrino energy

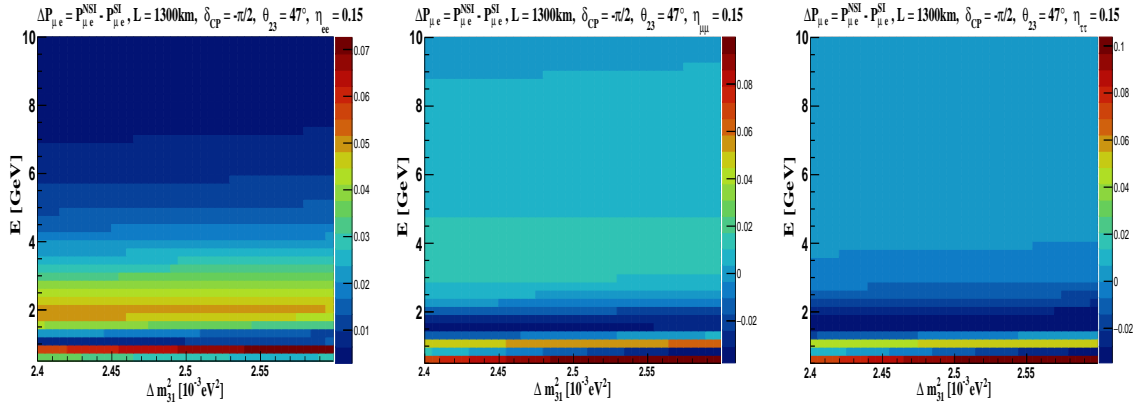


Figure 13: Variation of $\Delta P_{\mu e}$ in Δm_{31}^2 -E parameter space in the presence of scalar NSI elements η_{ee} (left-panel), $\eta_{\mu\mu}$ (middle-panel) and $\eta_{\tau\tau}$ (right-panel) for DUNE.

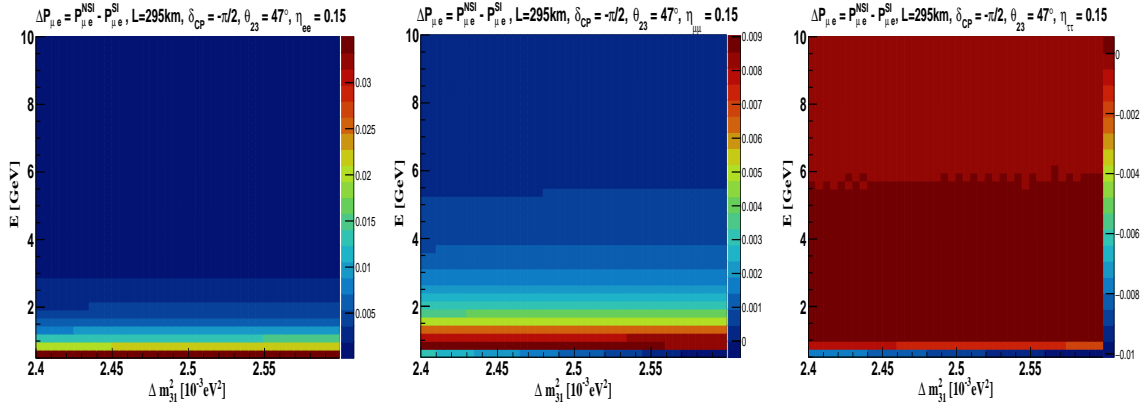


Figure 14: Variation of $\Delta P_{\mu e}$ in Δm_{31}^2 -E parameter space in the presence of scalar NSI elements η_{ee} (left-panel), $\eta_{\mu\mu}$ (middle-panel) and $\eta_{\tau\tau}$ (right-panel) for HK.

and Δm_{31}^2 for true NO. We have shown the variation in the presence of scalar NSI for

all the considered experiments i.e. DUNE, HK and HK+KNO. We consider the diagonal scalar NSI parameters i.e. η_{ee} (left-panel), $\eta_{\mu\mu}$ (middle-panel) and $\eta_{\tau\tau}$ (right-panel), one element a time. In figure 13, 14 and 15, we have shown the variation of $\Delta P_{\mu e}$ at DUNE, HK and HK+KNO respectively. In all the figures, we have fixed the value of $\eta_{\alpha\beta}$ at 0.15. The other oscillation parameters are fixed at values shown in table 2.

We observe that for higher values of neutrino energies, the value of $\Delta P_{\mu e}$ changes in the complete Δm_{31}^2 range for DUNE, HK and HK+KNO. In the case of DUNE, the same trend is seen in the presence of all scalar NSI parameters. In case of HK & HK+KNO, the impact on $\Delta P_{\mu e}$ is more prominent in the presence of η_{ee} in comparison to $\eta_{\mu\mu}$ and $\eta_{\tau\tau}$. For a fixed value of energy, $\Delta P_{\mu e}$ remains almost the same for the whole Δm_{31}^2 range.

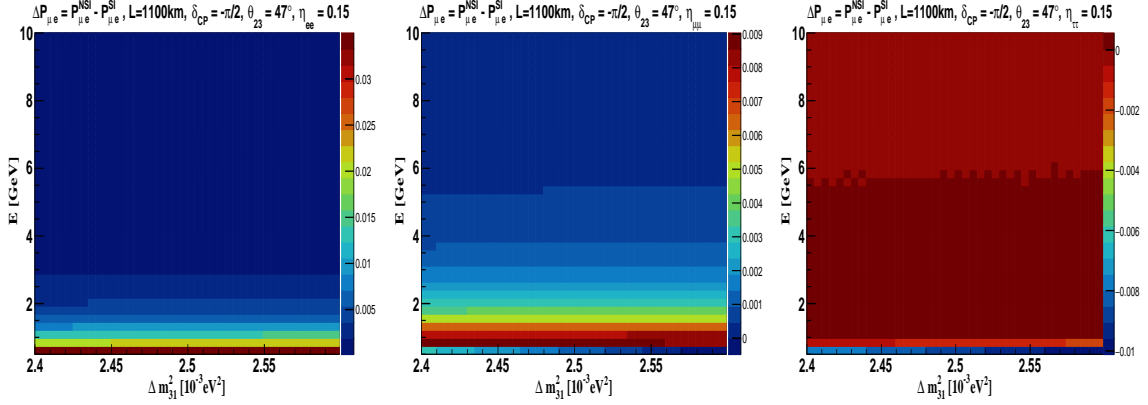


Figure 15: Variation of $\Delta P_{\mu e}$ in Δm_{31}^2 -E parameter space in the presence of scalar NSI elements η_{ee} (left-panel), $\eta_{\mu\mu}$ (middle-panel) and $\eta_{\tau\tau}$ (right-panel) for HK+KNO.

A.3 Impact of different fixed values of Δm_{31}^2 on the MO sensitivities

We have also explored the impact of different fixed values of Δm_{31}^2 on the MO sensitivities. In figure 16, we have examined how different true values of Δm_{31}^2 can affect the MO sensitivities for DUNE+HK configuration in the presence of η_{ee} . We have fixed the value of η_{ee} at 0.1 and the oscillation parameters as described in the manuscript. The left panel represents true NO whereas, the right panel represents true IO. In our analysis, we have kept the value of $|\Delta m_{31}^2|$ fixed for given mass ordering.

References

- [1] **SNO** Collaboration, Q. R. Ahmad et al., *Direct evidence for neutrino flavor transformation from neutral current interactions in the Sudbury Neutrino Observatory*, *Phys. Rev. Lett.* **89** (2002) 011301, [[nucl-ex/0204008](#)].
- [2] **Super-Kamiokande** Collaboration, Y. Fukuda et al., *Evidence for oscillation of atmospheric neutrinos*, *Phys. Rev. Lett.* **81** (1998) 1562–1567, [[hep-ex/9807003](#)].
- [3] J. Liao, D. Marfatia, and K. Whisnant, *Nonstandard neutrino interactions at DUNE, T2HK and T2HKK*, *JHEP* **01** (2017) 071, [[arXiv:1612.01443](#)].

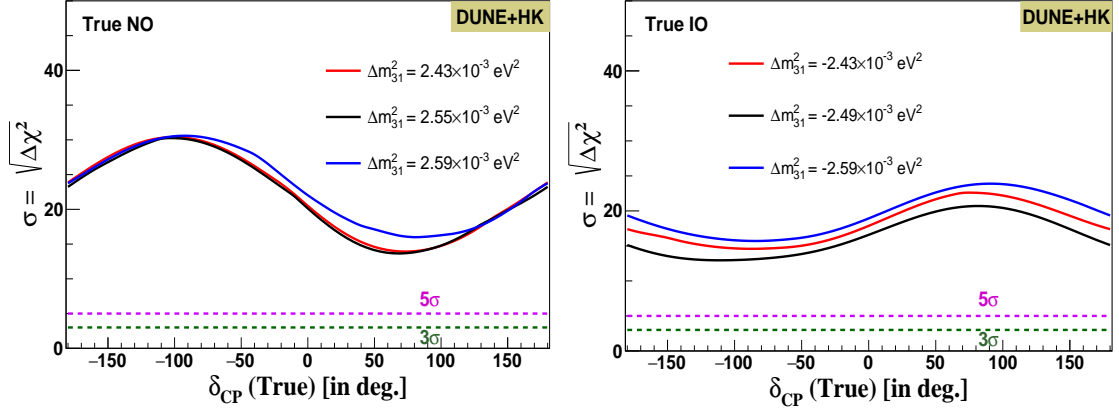


Figure 16: Impact of Δm_{31}^2 on the MO sensitivities for DUNE+HK configuration in the presence of η_{ee} fixed at 0.1. The left panel represents true NO and the right panel represents true IO.

- [4] A. Friedland and I. M. Shoemaker, *Searching for Novel Neutrino Interactions at NOvA and Beyond in Light of Large θ_{13}* , [arXiv:1207.6642](#).
- [5] J. A. B. Coelho, T. Kafka, W. A. Mann, J. Schneps, and O. Altinok, *Constraints for non-standard interaction $\epsilon_{e\tau}V_e$ from ν_e appearance in MINOS and T2K*, *Phys. Rev. D* **86** (2012) 113015, [[arXiv:1209.3757](#)].
- [6] Z. Rahman, A. Dasgupta, and R. Adhikari, *The Discovery reach of CP violation in neutrino oscillation with non-standard interaction effects*, *J. Phys. G* **42** (2015) 065001, [[arXiv:1503.03248](#)].
- [7] P. Coloma, *Non-Standard Interactions in propagation at the Deep Underground Neutrino Experiment*, *JHEP* **03** (2016) 016, [[arXiv:1511.06357](#)].
- [8] A. de Gouvêa and K. J. Kelly, *Non-standard Neutrino Interactions at DUNE*, *Nucl. Phys. B* **908** (2016) 318–335, [[arXiv:1511.05562](#)].
- [9] J. Liao, D. Marfatia, and K. Whisnant, *Degeneracies in long-baseline neutrino experiments from nonstandard interactions*, *Phys. Rev. D* **93** (2016), no. 9 093016, [[arXiv:1601.00927](#)].
- [10] D. V. Forero and P. Huber, *Hints for leptonic CP violation or New Physics?*, *Phys. Rev. Lett.* **117** (2016), no. 3 031801, [[arXiv:1601.03736](#)].
- [11] K. Huitu, T. J. Kärkkäinen, J. Maalampi, and S. Vihonen, *Constraining the nonstandard interaction parameters in long baseline neutrino experiments*, *Phys. Rev. D* **93** (2016), no. 5 053016, [[arXiv:1601.07730](#)].
- [12] P. Bakhti and Y. Farzan, *CP-Violation and Non-Standard Interactions at the MOMENT*, *JHEP* **07** (2016) 109, [[arXiv:1602.07099](#)].
- [13] A. Kumar, A. Khatun, S. K. Agarwalla, and A. Dighe, *A New Approach to Probe Non-Standard Interactions in Atmospheric Neutrino Experiments*, *JHEP* **04** (2021) 159, [[arXiv:2101.02607](#)].
- [14] S. K. Agarwalla, Y. Kao, D. Saha, and T. Takeuchi, *Running of Oscillation Parameters in Matter with Flavor-Diagonal Non-Standard Interactions of the Neutrino*, *JHEP* **11** (2015) 035, [[arXiv:1506.08464](#)].

- [15] S. K. Agarwalla, P. Bagchi, D. V. Forero, and M. Tórtola, *Probing Non-Standard Interactions at Daya Bay*, *JHEP* **07** (2015) 060, [[arXiv:1412.1064](#)].
- [16] S. K. Agarwalla, F. Lombardi, and T. Takeuchi, *Constraining Non-Standard Interactions of the Neutrino with Borexino*, *JHEP* **12** (2012) 079, [[arXiv:1207.3492](#)].
- [17] M. Blennow, S. Choubey, T. Ohlsson, D. Pramanik, and S. K. Raut, *A combined study of source, detector and matter non-standard neutrino interactions at DUNE*, *JHEP* **08** (2016) 090, [[arXiv:1606.08851](#)].
- [18] M. Blennow, S. Choubey, T. Ohlsson, and S. K. Raut, *Exploring Source and Detector Non-Standard Neutrino Interactions at ESS ν SB*, *JHEP* **09** (2015) 096, [[arXiv:1507.02868](#)].
- [19] K. N. Deepthi, S. Goswami, and N. Nath, *Can nonstandard interactions jeopardize the hierarchy sensitivity of DUNE?*, *Phys. Rev. D* **96** (2017), no. 7 075023, [[arXiv:1612.00784](#)].
- [20] M. Masud, P. Mehta, C. A. Ternes, and M. Tortola, *Non-standard neutrino oscillations: perspective from unitarity triangles*, *JHEP* **05** (2021) 171, [[arXiv:2103.11143](#)].
- [21] C. Soumya, M. Ghosh, S. K. Raut, N. Sinha, and P. Mehta, *Probing muonic charged current nonstandard interactions at decay-at-rest facilities in conjunction with T2HK*, *Phys. Rev. D* **101** (2020), no. 5 055009, [[arXiv:1911.05021](#)].
- [22] M. Masud, S. Roy, and P. Mehta, *Correlations and degeneracies among the NSI parameters with tunable beams at DUNE*, *Phys. Rev. D* **99** (2019), no. 11 115032, [[arXiv:1812.10290](#)].
- [23] M. Masud and P. Mehta, *Imprint of non-standard interactions on the CP violation measurements at long baseline experiments*, *Pramana* **89** (2017), no. 4 62.
- [24] M. Masud, A. Chatterjee, and P. Mehta, *Probing CP violation signal at DUNE in presence of non-standard neutrino interactions*, *J. Phys. G* **43** (2016), no. 9 095005, [[arXiv:1510.08261](#)].
- [25] S.-F. Ge and A. Y. Smirnov, *Non-standard interactions and the CP phase measurements in neutrino oscillations at low energies*, *JHEP* **10** (2016) 138, [[arXiv:1607.08513](#)].
- [26] S. Fukasawa, M. Ghosh, and O. Yasuda, *Sensitivity of the T2HKK experiment to nonstandard interactions*, *Phys. Rev. D* **95** (2017), no. 5 055005, [[arXiv:1611.06141](#)].
- [27] S. S. Chatterjee, P. S. B. Dev, and P. A. N. Machado, *Impact of improved energy resolution on DUNE sensitivity to neutrino non-standard interactions*, *JHEP* **08** (2021) 163, [[arXiv:2106.04597](#)].
- [28] A. Medhi, A. Sarker, and M. M. Devi, *Scalar NSI: A unique tool for constraining absolute neutrino masses via ν -oscillations*, [arXiv:2307.05348](#).
- [29] M. E. Chaves, P. C. de Holanda, and O. L. G. Peres, *Testing non-standard neutrino interactions in (anti)-electron neutrino disappearance experiments*, *JHEP* **03** (2023) 180, [[arXiv:2106.15725](#)].
- [30] B. Brahma and A. Giri, *Discernible NSI Effects in Long-Baseline Neutrino Experiments*, [arXiv:2302.09592](#).
- [31] H. Davoudiasl and P. B. Denton, *Sterile neutrino shape shifting caused by dark matter*, *Phys. Rev. D* **108** (2023), no. 3 035013, [[arXiv:2301.09651](#)].
- [32] S. S. Chatterjee and A. Palazzo, *Nonstandard Neutrino Interactions as a Solution to the NO ν A and T2K Discrepancy*, *Phys. Rev. Lett.* **126** (2021), no. 5 051802, [[arXiv:2008.04161](#)].

- [33] S. Choubey and T. Ohlsson, *Bounds on Non-Standard Neutrino Interactions Using PINGU*, *Phys. Lett. B* **739** (2014) 357–364, [[arXiv:1410.0410](#)].
- [34] D. K. Singha, M. Ghosh, R. Majhi, and R. Mohanta, *Optimal configuration of Protvino to ORCA experiment for hierarchy and non-standard interactions*, *JHEP* **05** (2022) 117, [[arXiv:2112.04876](#)].
- [35] P. B. Denton, Y. Farzan, and I. M. Shoemaker, *Testing large non-standard neutrino interactions with arbitrary mediator mass after COHERENT data*, *JHEP* **07** (2018) 037, [[arXiv:1804.03660](#)].
- [36] P. B. Denton, J. Gehrlein, and R. Pestes, *CP -Violating Neutrino Nonstandard Interactions in Long-Baseline-Accelerator Data*, *Phys. Rev. Lett.* **126** (2021), no. 5 051801, [[arXiv:2008.01110](#)].
- [37] Y. Farzan and I. M. Shoemaker, *Lepton Flavor Violating Non-Standard Interactions via Light Mediators*, *JHEP* **07** (2016) 033, [[arXiv:1512.09147](#)].
- [38] V. A. Kostelecky and M. Mewes, *Lorentz and CPT violation in neutrinos*, *Phys. Rev. D* **69** (2004) 016005, [[hep-ph/0309025](#)].
- [39] **SNO** Collaboration, B. Aharmim et al., *Tests of Lorentz invariance at the Sudbury Neutrino Observatory*, *Phys. Rev. D* **98** (2018), no. 11 112013, [[arXiv:1811.00166](#)].
- [40] M. Mewes, *Signals for Lorentz violation in gravitational waves*, *Phys. Rev. D* **99** (2019), no. 10 104062, [[arXiv:1905.00409](#)].
- [41] Y. Huang, H. Li, and B.-Q. Ma, *Consistent Lorentz violation features from near-TeV IceCube neutrinos*, *Phys. Rev. D* **99** (2019), no. 12 123018, [[arXiv:1906.07329](#)].
- [42] P. Arias, J. Gamboa, F. Méndez, A. Das, and J. López-Sarrión, *Cpt/lorentz invariance violation and neutrino oscillation*, *Physics Letters B* **650** (2007), no. 5 401–406.
- [43] **LSND** Collaboration, L. B. Auerbach et al., *Tests of Lorentz violation in anti- $\nu(\mu) \rightarrow$ anti- $\nu(e)$ oscillations*, *Phys. Rev. D* **72** (2005) 076004, [[hep-ex/0506067](#)].
- [44] **MINOS** Collaboration, P. Adamson et al., *Testing Lorentz Invariance and CPT Conservation with NuMI Neutrinos in the MINOS Near Detector*, *Phys. Rev. Lett.* **101** (2008) 151601, [[arXiv:0806.4945](#)].
- [45] **MINOS** Collaboration, P. Adamson et al., *A Search for Lorentz Invariance and CPT Violation with the MINOS Far Detector*, *Phys. Rev. Lett.* **105** (2010) 151601, [[arXiv:1007.2791](#)].
- [46] **IceCube** Collaboration, R. Abbasi et al., *Search for a Lorentz-violating sidereal signal with atmospheric neutrinos in IceCube*, *Phys. Rev. D* **82** (2010) 112003, [[arXiv:1010.4096](#)].
- [47] **MiniBooNE** Collaboration, A. A. Aguilar-Arevalo et al., *Test of Lorentz and CPT violation with Short Baseline Neutrino Oscillation Excesses*, *Phys. Lett. B* **718** (2013) 1303–1308, [[arXiv:1109.3480](#)].
- [48] **Double Chooz** Collaboration, Y. Abe et al., *First Test of Lorentz Violation with a Reactor-based Antineutrino Experiment*, *Phys. Rev. D* **86** (2012) 112009, [[arXiv:1209.5810](#)].
- [49] A. Sarker, A. Medhi, and M. M. Devi, *Investigating the effects of Lorentz Invariance Violation on the CP-sensitivities of the Deep Underground Neutrino Experiment*, *Eur. Phys. J. C* **83** (2023), no. 7 592, [[arXiv:2302.10456](#)].

- [50] T. Sarkar, *Probing non-unitarity of neutrino mixing in the scenario of Lorentz violation and dark nonstandard interaction*, [arXiv:2209.10233](#).
- [51] R. Majhi, D. K. Singha, M. Ghosh, and R. Mohanta, *Distinguishing nonstandard interaction and Lorentz invariance violation at the Protvino to super-ORCA experiment*, *Phys. Rev. D* **107** (2023), no. 7 075036, [[arXiv:2212.07244](#)].
- [52] J. M. Berryman, A. de Gouvea, and D. Hernandez, *Solar Neutrinos and the Decaying Neutrino Hypothesis*, *Phys. Rev. D* **92** (2015), no. 7 073003, [[arXiv:1411.0308](#)].
- [53] R. Picoreti, M. Guzzo, P. de Holanda, and O. Peres, *Neutrino decay and solar neutrino seasonal effect*, *Physics Letters B* **761** (2016) 70–73.
- [54] **SNO** Collaboration, B. Aharmim et al., *Constraints on Neutrino Lifetime from the Sudbury Neutrino Observatory*, *Phys. Rev. D* **99** (2019), no. 3 032013, [[arXiv:1812.01088](#)].
- [55] R. Gomes, A. Gomes, and O. Peres, *Constraints on neutrino decay lifetime using long-baseline charged and neutral current data*, *Physics Letters B* **740** (2015) 345–352.
- [56] P. Coloma and O. L. G. Peres, *Visible neutrino decay at DUNE*, [arXiv:1705.03599](#).
- [57] T. Abrahão, H. Minakata, H. Nunokawa, and A. A. Quiroga, *Constraint on Neutrino Decay with Medium-Baseline Reactor Neutrino Oscillation Experiments*, *JHEP* **11** (2015) 001, [[arXiv:1506.02314](#)].
- [58] Y. Liu, L. Hu, and M.-L. Ge, *Effect of violation of quantum mechanics on neutrino oscillation*, *Phys. Rev. D* **56** (Nov, 1997) 6648–6652.
- [59] F. Benatti and R. Floreanini, *Open system approach to neutrino oscillations*, *JHEP* **02** (2000) 032, [[hep-ph/0002221](#)].
- [60] G. B. Gomes, D. V. Forero, M. M. Guzzo, P. C. de Holanda, and R. L. N. Oliveira, *Quantum decoherence effects in neutrino oscillations at dune*, *Phys. Rev. D* **100** (Sep, 2019) 055023.
- [61] G. Balieiro Gomes, M. M. Guzzo, P. C. de Holanda, and R. L. N. Oliveira, *Parameter limits for neutrino oscillation with decoherence in kamland*, *Phys. Rev. D* **95** (Jun, 2017) 113005.
- [62] E. Lisi, A. Marrone, and D. Montanino, *Probing possible decoherence effects in atmospheric neutrino oscillations*, *Phys. Rev. Lett.* **85** (2000) 1166–1169, [[hep-ph/0002053](#)].
- [63] P. B. Denton, *A Return To Neutrino Normalcy*, [arXiv:2003.04319](#).
- [64] P. B. Denton and S. J. Parke, *Parameter symmetries of neutrino oscillations in vacuum, matter, and approximation schemes*, *Phys. Rev. D* **105** (2022), no. 1 013002, [[arXiv:2106.12436](#)].
- [65] A. de Gouvea and J. Jenkins, *The Physical Range of Majorana Neutrino Mixing Parameters*, *Phys. Rev. D* **78** (2008) 053003, [[arXiv:0804.3627](#)].
- [66] **SNO** Collaboration, Q. R. Ahmad et al., *Measurement of the rate of $\nu_e + d \rightarrow p + p + e^-$ interactions produced by ^8B solar neutrinos at the Sudbury Neutrino Observatory*, *Phys. Rev. Lett.* **87** (2001) 071301, [[nucl-ex/0106015](#)].
- [67] **SNO** Collaboration, Q. R. Ahmad et al., *Measurement of day and night neutrino energy spectra at SNO and constraints on neutrino mixing parameters*, *Phys. Rev. Lett.* **89** (2002) 011302, [[nucl-ex/0204009](#)].
- [68] P. F. Harrison, D. H. Perkins, and W. G. Scott, *Tri-bimaximal mixing and the neutrino oscillation data*, *Phys. Lett. B* **530** (2002) 167, [[hep-ph/0202074](#)].

- [69] I. Esteban, M. C. Gonzalez-Garcia, M. Maltoni, T. Schwetz, and A. Zhou, *The fate of hints: updated global analysis of three-flavor neutrino oscillations*, *JHEP* **09** (2020) 178, [[arXiv:2007.14792](#)].
- [70] P. Alivisatos et al., *KamLAND: A Liquid scintillator anti-neutrino detector at the Kamioka site*, .
- [71] B. T. Cleveland, T. Daily, R. Davis, Jr., J. R. Distel, K. Lande, C. K. Lee, P. S. Wildenhain, and J. Ullman, *Measurement of the solar electron neutrino flux with the Homestake chlorine detector*, *Astrophys. J.* **496** (1998) 505–526.
- [72] **SAGE** Collaboration, J. N. Abdurashitov et al., *Measurement of the solar neutrino capture rate with gallium metal*, *Phys. Rev. C* **60** (1999) 055801, [[astro-ph/9907113](#)].
- [73] **Bugey**, **Galex** Collaboration, R. Aleksan, J. Bouchez, M. Cribier, E. Kajfasz, B. Pichard, F. Pierre, J. Poinignon, M. Spiro, and J. F. Thomas, *Measurement of Fast Neutrons in the Gran Sasso Laboratory Using a ^6Li Doped Liquid Scintillator*, *Nucl. Instrum. Meth. A* **274** (1989) 203.
- [74] G. Bellini et al., *Precision measurement of the ^7Be solar neutrino interaction rate in Borexino*, *Phys. Rev. Lett.* **107** (2011) 141302, [[arXiv:1104.1816](#)].
- [75] **ICAL** Collaboration, S. Ahmed et al., *Physics Potential of the ICAL detector at the India-based Neutrino Observatory (INO)*, *Pramana* **88** (2017), no. 5 79, [[arXiv:1505.07380](#)].
- [76] **IceCube-PINGU** Collaboration, M. G. Aartsen et al., *Letter of Intent: The Precision IceCube Next Generation Upgrade (PINGU)*, [arXiv:1401.2046](#).
- [77] **Super-Kamiokande** Collaboration, Y. Fukuda et al., *The Super-Kamiokande detector*, *Nucl. Instrum. Meth. A* **501** (2003) 418–462.
- [78] **KM3Net** Collaboration, S. Adrian-Martinez et al., *Letter of intent for KM3NeT 2.0*, *J. Phys. G* **43** (2016), no. 8 084001, [[arXiv:1601.07459](#)].
- [79] **IceCube-Gen2** Collaboration, M. G. Aartsen et al., *IceCube-Gen2: the window to the extreme Universe*, *J. Phys. G* **48** (2021), no. 6 060501, [[arXiv:2008.04323](#)].
- [80] F. Ardellier et al., *Letter of intent for Double-CHOOZ: A Search for the mixing angle $\theta(13)$* , [hep-ex/0405032](#).
- [81] **RENO** Collaboration, J. K. Ahn et al., *RENO: An Experiment for Neutrino Oscillation Parameter θ_{13} Using Reactor Neutrinos at Yonggwang*, [arXiv:1003.1391](#).
- [82] **Daya Bay** Collaboration, X. Guo et al., *A Precision measurement of the neutrino mixing angle θ_{13} using reactor antineutrinos at Daya-Bay*, [hep-ex/0701029](#).
- [83] **JUNO** Collaboration, A. Abusleme et al., *JUNO physics and detector*, *Prog. Part. Nucl. Phys.* **123** (2022) 103927, [[arXiv:2104.02565](#)].
- [84] **NOvA** Collaboration, D. S. Ayres et al., *NOvA: Proposal to Build a 30 Kiloton Off-Axis Detector to Study $\nu_\mu \rightarrow \nu_e$ Oscillations in the NuMI Beamline*, [hep-ex/0503053](#).
- [85] **T2K** Collaboration, Y. Itow et al., *The JHF-Kamioka neutrino project*, in *3rd Workshop on Neutrino Oscillations and Their Origin (NOON 2001)*, pp. 239–248, 6, 2001. [hep-ex/0106019](#).
- [86] **DUNE** Collaboration, B. Abi et al., *Deep Underground Neutrino Experiment (DUNE)*, *Far*

Detector Technical Design Report, Volume IV Far Detector Single-phase Technology, JINST **15** (2020), no. 08 T08010, [[arXiv:2002.03010](#)].

- [87] **Hyper-Kamiokande Proto-** Collaboration, K. Abe et al., *Physics potential of a long-baseline neutrino oscillation experiment using a J-PARC neutrino beam and Hyper-Kamiokande*, *PTEP* **2015** (2015) 053C02, [[arXiv:1502.05199](#)].
- [88] **Hyper-Kamiokande** Collaboration, K. Abe et al., *Physics potentials with the second Hyper-Kamiokande detector in Korea*, *PTEP* **2018** (2018), no. 6 063C01, [[arXiv:1611.06118](#)].
- [89] **ESSnuSB** Collaboration, E. Baussan et al., *A very intense neutrino super beam experiment for leptonic CP violation discovery based on the European spallation source linac*, *Nucl. Phys. B* **885** (2014) 127–149, [[arXiv:1309.7022](#)].
- [90] A. V. Akindinov et al., *Letter of Interest for a Neutrino Beam from Protvino to KM3NeT/ORCA*, *Eur. Phys. J. C* **79** (2019), no. 9 758, [[arXiv:1902.06083](#)].
- [91] **JUNO** Collaboration, F. An et al., *Neutrino Physics with JUNO*, *J. Phys. G* **43** (2016), no. 3 030401, [[arXiv:1507.05613](#)].
- [92] M. M. Devi, T. Thakore, S. K. Agarwalla, and A. Dighe, *Enhancing sensitivity to neutrino parameters at INO combining muon and hadron information*, *JHEP* **10** (2014) 189, [[arXiv:1406.3689](#)].
- [93] **DUNE** Collaboration, B. Abi et al., *Long-baseline neutrino oscillation physics potential of the DUNE experiment*, *Eur. Phys. J. C* **80** (2020), no. 10 978, [[arXiv:2006.16043](#)].
- [94] **ESSnuSB** Collaboration, A. Alekou et al., *Updated physics performance of the ESSnuSB experiment: ESSnuSB collaboration*, *Eur. Phys. J. C* **81** (2021), no. 12 1130, [[arXiv:2107.07585](#)].
- [95] H. Nunokawa, S. J. Parke, and R. Zukanovich Funchal, *Another possible way to determine the neutrino mass hierarchy*, *Phys. Rev. D* **72** (2005) 013009, [[hep-ph/0503283](#)].
- [96] K. Chakraborty, S. Goswami, C. Gupta, and T. Thakore, *Enhancing the hierarchy and octant sensitivity of ESSnuSB in conjunction with T2K, NOvA and ICAL@INO*, *JHEP* **05** (2019) 137, [[arXiv:1902.02963](#)].
- [97] S. Cao, A. Nath, T. V. Ngoc, P. T. Quyen, N. T. Hong Van, and N. K. Francis, *Physics potential of the combined sensitivity of T2K-II, NOvA extension, and JUNO*, *Phys. Rev. D* **103** (2021), no. 11 112010, [[arXiv:2009.08585](#)].
- [98] A. Ghosh, T. Thakore, and S. Choubey, *Determining the Neutrino Mass Hierarchy with INO, T2K, NOvA and Reactor Experiments*, *JHEP* **04** (2013) 009, [[arXiv:1212.1305](#)].
- [99] **IceCube-Gen2** Collaboration, M. G. Aartsen et al., *Combined sensitivity to the neutrino mass ordering with JUNO, the IceCube Upgrade, and PINGU*, *Phys. Rev. D* **101** (2020), no. 3 032006, [[arXiv:1911.06745](#)].
- [100] S. Choubey, M. Ghosh, and D. Raikwal, *Neutrino Mass Ordering - Circumventing the Challenges using Synergy between T2HK and JUNO*, [[arXiv:2207.04784](#)].
- [101] D. Raikwal, S. Choubey, and M. Ghosh, *Neutrino Mass Ordering Using Synergy between ICAL, T2HK, and JUNO*, *LHEP* **2023** (2023) 376.
- [102] F. Capozzi, S. S. Chatterjee, and A. Palazzo, *Neutrino Mass Ordering Obscured by Nonstandard Interactions*, *Phys. Rev. Lett.* **124** (2020), no. 11 111801, [[arXiv:1908.06992](#)].

- [103] I. Esteban, M. C. Gonzalez-Garcia, and M. Maltoni, *On the Determination of Leptonic CP Violation and Neutrino Mass Ordering in Presence of Non-Standard Interactions: Present Status*, *JHEP* **06** (2019) 055, [[arXiv:1905.05203](#)].
- [104] M. Masud and P. Mehta, *Nonstandard interactions and resolving the ordering of neutrino masses at DUNE and other long baseline experiments*, *Phys. Rev. D* **94** (2016), no. 5 053007, [[arXiv:1606.05662](#)].
- [105] P. Coloma and T. Schwetz, *Generalized mass ordering degeneracy in neutrino oscillation experiments*, *Phys. Rev. D* **94** (2016), no. 5 055005, [[arXiv:1604.05772](#)]. [Erratum: *Phys.Rev.D* 95, 079903 (2017)].
- [106] P. Bakhti and Y. Farzan, *Shedding light on LMA-Dark solar neutrino solution by medium baseline reactor experiments: JUNO and RENO-50*, *JHEP* **07** (2014) 064, [[arXiv:1403.0744](#)].
- [107] A. de Gouvea, A. Friedland, and H. Murayama, *The Dark side of the solar neutrino parameter space*, *Phys. Lett. B* **490** (2000) 125–130, [[hep-ph/0002064](#)].
- [108] P. B. Denton and J. Gehrlein, *New constraints on the dark side of non-standard interactions from reactor neutrino scattering data*, *Phys. Rev. D* **106** (2022), no. 1 015022, [[arXiv:2204.09060](#)].
- [109] D. Dutta, P. Ghoshal, and S. Roy, *Effect of Non Unitarity on Neutrino Mass Hierarchy determination at DUNE, NO ν A and T2K*, *Nucl. Phys. B* **920** (2017) 385–401, [[arXiv:1609.07094](#)].
- [110] S. Choubey, D. Dutta, and D. Pramanik, *Imprints of a light Sterile Neutrino at DUNE, T2HK and T2HKK*, *Phys. Rev. D* **96** (2017), no. 5 056026, [[arXiv:1704.07269](#)].
- [111] S.-F. Ge and S. J. Parke, *Scalar Nonstandard Interactions in Neutrino Oscillation*, *Phys. Rev. Lett.* **122** (2019), no. 21 211801, [[arXiv:1812.08376](#)].
- [112] Y. Yang and J. P. Kneller, *Neutrino flavor transformation in supernovae as a probe for nonstandard neutrino-scalar interactions*, *Phys. Rev. D* **97** (2018), no. 10 103018, [[arXiv:1803.04504](#)].
- [113] A. N. Khan, W. Rodejohann, and X.-J. Xu, *Borexino and general neutrino interactions*, *Phys. Rev. D* **101** (2020), no. 5 055047, [[arXiv:1906.12102](#)].
- [114] A. Gupta, D. Majumdar, and S. Prakash, *Neutrino oscillation measurements with JUNO in the presence of scalar NSI*, [arXiv:2306.07343](#).
- [115] K. S. Babu, G. Chauhan, and P. S. Bhupal Dev, *Neutrino nonstandard interactions via light scalars in the Earth, Sun, supernovae, and the early Universe*, *Phys. Rev. D* **101** (2020), no. 9 095029, [[arXiv:1912.13488](#)].
- [116] J. Venzor, A. Pérez-Lorezana, and J. De-Santiago, *Bounds on neutrino-scalar nonstandard interactions from big bang nucleosynthesis*, *Phys. Rev. D* **103** (2021), no. 4 043534, [[arXiv:2009.08104](#)].
- [117] A. Medhi, D. Dutta, and M. M. Devi, *Exploring the effects of scalar non standard interactions on the CP violation sensitivity at DUNE*, *JHEP* **06** (2022) 129, [[arXiv:2111.12943](#)].
- [118] A. Medhi, M. M. Devi, and D. Dutta, *Imprints of scalar NSI on the CP-violation sensitivity using synergy among DUNE, T2HK and T2HKK*, *JHEP* **01** (2023) 079, [[arXiv:2209.05287](#)].

- [119] P. B. Denton, A. Giarnetti, and D. Meloni, *How to identify different new neutrino oscillation physics scenarios at DUNE*, *JHEP* **02** (2023) 210, [[arXiv:2210.00109](#)].
- [120] D. K. Singha, R. Majhi, L. Panda, M. Ghosh, and R. Mohanta, *Study of Scalar Non Standard Interaction at Protvino to Super-ORCA experiment*, [arXiv:2308.10789](#).
- [121] J. Linder, *Derivation of neutrino matter potentials induced by earth*, [hep-ph/0504264](#).
- [122] L. Wolfenstein, *Neutrino Oscillations in Matter*, *Phys. Rev. D* **17** (1978) 2369–2374.
- [123] J. F. Nieves and P. B. Pal, *Generalized Fierz identities*, *Am. J. Phys.* **72** (2004) 1100–1108, [[hep-ph/0306087](#)].
- [124] C. C. Nishi, *Simple derivation of general Fierz-like identities*, *Am. J. Phys.* **73** (2005) 1160–1163, [[hep-ph/0412245](#)].
- [125] Z. Maki, M. Nakagawa, and S. Sakata, *Remarks on the unified model of elementary particles*, *Prog. Theor. Phys.* **28** (1962) 870–880.
- [126] S. M. Bilenky and S. T. Petcov, *Massive Neutrinos and Neutrino Oscillations*, *Rev. Mod. Phys.* **59** (1987) 671. [Erratum: *Rev. Mod. Phys.* 61, 169 (1989), Erratum: *Rev. Mod. Phys.* 60, 575–575 (1988)].
- [127] B. Pontecorvo, *Mesonium and anti-mesonium*, *Sov. Phys. JETP* **6** (1957) 429.
- [128] B. Pontecorvo, *Inverse beta processes and nonconservation of lepton charge*, *Zh. Eksp. Teor. Fiz.* **34** (1957) 247.
- [129] B. Pontecorvo, *Neutrino Experiments and the Problem of Conservation of Leptonic Charge*, *Zh. Eksp. Teor. Fiz.* **53** (1967) 1717–1725.
- [130] **Particle Data Group** Collaboration, P. A. Zyla et al., *Review of Particle Physics*, *PTEP* **2020** (2020), no. 8 083C01.
- [131] P. Huber, M. Lindner, and W. Winter, *Simulation of long-baseline neutrino oscillation experiments with GLoBES (General Long Baseline Experiment Simulator)*, *Comput. Phys. Commun.* **167** (2005) 195, [[hep-ph/0407333](#)].
- [132] J. Kopp, *Efficient numerical diagonalization of hermitian 3×3 matrices*, *Int. J. Mod. Phys. C* **19** (2008) 523–548, [[physics/0610206](#)].
- [133] P. Huber, J. Kopp, M. Lindner, M. Rolinec, and W. Winter, *New features in the simulation of neutrino oscillation experiments with GLoBES 3.0: General Long Baseline Experiment Simulator*, *Comput. Phys. Commun.* **177** (2007) 432–438, [[hep-ph/0701187](#)].
- [134] I. Esteban, M. C. Gonzalez-Garcia, M. Maltoni, T. Schwetz, and A. Zhou, *The fate of hints: updated global analysis of three-flavor neutrino oscillations*, *JHEP* **09** (2020) 178, [[arXiv:2007.14792](#)].
- [135] G. L. Fogli, E. Lisi, A. Marrone, D. Montanino, and A. Palazzo, *Getting the most from the statistical analysis of solar neutrino oscillations*, *Phys. Rev. D* **66** (2002) 053010, [[hep-ph/0206162](#)].
- [136] **Planck** Collaboration, N. Aghanim et al., *Planck 2018 results. VI. Cosmological parameters*, *Astron. Astrophys.* **641** (2020) A6, [[arXiv:1807.06209](#)]. [Erratum: *Astron. Astrophys.* 652, C4 (2021)].
- [137] **DUNE** Collaboration, R. Acciarri et al., *Long-Baseline Neutrino Facility (LBNF) and Deep Underground Neutrino Experiment (DUNE): Conceptual Design Report, Volume 1: The LBNF and DUNE Projects*, [arXiv:1601.05471](#).

- [138] **DUNE** Collaboration, R. Acciarri et al., *Long-Baseline Neutrino Facility (LBNF) and Deep Underground Neutrino Experiment (DUNE): Conceptual Design Report, Volume 2: The Physics Program for DUNE at LBNF*, [arXiv:1512.06148](#).
- [139] **DUNE** Collaboration, R. Acciarri et al., *Long-Baseline Neutrino Facility (LBNF) and Deep Underground Neutrino Experiment (DUNE): Conceptual Design Report, Volume 4 The DUNE Detectors at LBNF*, [arXiv:1601.02984](#).
- [140] **DUNE** Collaboration, B. Abi et al., *Deep Underground Neutrino Experiment (DUNE), Far Detector Technical Design Report, Volume II: DUNE Physics*, [arXiv:2002.03005](#).
- [141] **DUNE** Collaboration, V. Hewes et al., *Deep Underground Neutrino Experiment (DUNE) Near Detector Conceptual Design Report, Instruments* **5** (2021), no. 4 31, [[arXiv:2103.13910](#)].